The laser-plasma surface interaction: towards attosecond sources of light

Robin Timmis

Your College
University of Oxford

A thesis submitted for the degree of
Doctor of Philosophy

Michaelmas 2014

Abstract

Your abstract text goes here. Check your departmental regulations, but generally this should be less than 300 words. See the beginning of Chapter **??** for more.

Lorem ipsum dolor sit amet, consectetur adipiscing elit. Pellentesque sit amet nibh volutpat, scelerisque nibh a, vehicula neque. Integer placerat nulla massa, et vestibulum velit dignissim id. Ut eget nisi elementum, consectetur nibh in, condimentum velit. Quisque sodales dui ut tempus mattis. Duis malesuada arcu at ligula egestas egestas. Phasellus interdum odio at sapien fringilla scelerisque. Mauris sagittis eleifend sapien, sit amet laoreet felis mollis quis. Pellentesque dui ante, finibus eget blandit sit amet, tincidunt eu neque. Vivamus rutrum dapibus ligula, ut imperdiet lectus tincidunt ac. Pellentesque ac lorem sed diam egestas lobortis.

Suspendisse leo purus, efficitur mattis urna a, maximus molestie nisl. Aenean porta semper tortor a vestibulum. Suspendisse viverra facilisis lorem, non pretium erat lacinia a. Vestibulum tempus, quam vitae placerat porta, magna risus euismod purus, in viverra lorem dui at metus. Sed ac sollicitudin nunc. In maximus ipsum nunc, placerat maximus tortor gravida varius. Suspendisse pretium, lorem at porttitor rhoncus, nulla urna condimentum tortor, sed suscipit nisi metus ac risus.

Aenean sit amet enim quis lorem tristique commodo vitae ut lorem. Duis vel tincidunt lacus. Sed massa velit, lacinia sed posuere vitae, malesuada vel ante. Praesent a rhoncus leo. Etiam sed rutrum enim. Pellentesque lobortis elementum augue, at suscipit justo malesuada at. Lorem ipsum dolor sit amet, consectetur adipiscing elit. Praesent rhoncus convallis ex. Etiam commodo nunc ex, non consequat diam consectetur ut. Pellentesque vitae est nec enim interdum dapibus. Donec dapibus purus ipsum, eget tincidunt ex gravida eget. Donec luctus nisi eu fringilla mollis. Donec eget lobortis diam.

Suspendisse finibus placerat dolor. Etiam ornare elementum ex ut vehicula. Donec accumsan mattis erat. Quisque cursus fringilla diam, eget placerat neque bibendum eu. Ut faucibus dui vitae dolor porta, at elementum ipsum semper. Sed ultrices dui non arcu pellentesque placerat. Etiam posuere malesuada turpis, nec malesuada tellus malesuada.

The laser-plasma surface interaction: towards attosecond sources of light

Robin Timmis

Your College

University of Oxford

A thesis submitted for the degree of

Doctor of Philosophy

Michaelmas 2014

Acknowledgements

Personal

This is where you thank your advisor, colleagues, and family and friends.

Lorem ipsum dolor sit amet, consectetur adipiscing elit. Vestibulum feugiat et est at accumsan. Praesent sed elit mattis, congue mi sed, porta ipsum. In non ullamcorper lacus. Quisque volutpat tempus ligula ac ultricies. Nam sed erat feugiat, elementum dolor sed, elementum neque. Aliquam eu iaculis est, a sollicitudin augue. Cras id lorem vel purus posuere tempor. Proin tincidunt, sapien non dictum aliquam, ex odio ornare mauris, ultrices viverra nisi magna in lacus. Fusce aliquet molestie massa, ut fringilla purus rutrum consectetur. Nam non nunc tincidunt, rutrum dui sit amet, ornare nunc. Donec cursus tortor vel odio molestie dignissim. Vivamus id mi erat. Duis porttitor diam tempor rutrum porttitor. Lorem ipsum dolor sit amet, consectetur adipiscing elit. Sed condimentum venenatis consectetur. Lorem ipsum dolor sit amet, consectetur adipiscing elit.

Aenean sit amet lectus nec tellus viverra ultrices vitae commodo nunc. Mauris at maximus arcu. Aliquam varius congue orci et ultrices. In non ipsum vel est scelerisque efficitur in at augue. Nullam rhoncus orci velit. Duis ultricies accumsan feugiat. Etiam consectetur ornare velit et eleifend.

Suspendisse sed enim lacinia, pharetra neque ac, ultricies urna. Phasellus sit amet cursus purus. Quisque non odio libero. Etiam iaculis odio a ex volutpat, eget pulvinar augue mollis. Mauris nibh lorem, mollis quis semper quis, consequat nec metus. Etiam dolor mi, cursus a ipsum aliquam, eleifend venenatis ipsum. Maecenas tempus, nibh eget scelerisque feugiat, leo nibh lobortis diam, id laoreet purus dolor eu mauris. Pellentesque habitant morbi tristique senectus et netus et malesuada fames ac turpis egestas. Nulla eget tortor eu arcu sagittis euismod fermentum id neque. In sit amet justo ligula. Donec rutrum ex a aliquet egestas.

Institutional

If you want to separate out your thanks for funding and institutional support, I don't think there's any rule against it. Of course, you could also just remove the subsections and do one big traditional acknowledgement section.

Lorem ipsum dolor sit amet, consectetur adipiscing elit. Ut luctus tempor ex at pretium. Sed varius, mauris at dapibus lobortis, elit purus tempor neque,

facilisis sollicitudin felis nunc a urna. Morbi mattis ante non augue blandit pulvinar. Quisque nec euismod mauris. Nulla et tellus eu nibh auctor malesuada quis imperdiet quam. Sed eget tincidunt velit. Cras molestie sem ipsum, at faucibus quam mattis vel. Quisque vel placerat orci, id tempor urna. Vivamus mollis, neque in aliquam consequat, dui sem volutpat lorem, sit amet tempor ipsum felis eget ante. Integer lacinia nulla vitae felis vulputate, at tincidunt ligula maximus. Aenean venenatis dolor ante, euismod ultrices nibh mollis ac. Ut malesuada aliquam urna, ac interdum magna malesuada posuere.

Abstract

Your abstract text goes here. Check your departmental regulations, but generally this should be less than 300 words. See the beginning of Chapter **??** for more.

Lorem ipsum dolor sit amet, consectetur adipiscing elit. Pellentesque sit amet nibh volutpat, scelerisque nibh a, vehicula neque. Integer placerat nulla massa, et vestibulum velit dignissim id. Ut eget nisi elementum, consectetur nibh in, condimentum velit. Quisque sodales dui ut tempus mattis. Duis malesuada arcu at ligula egestas egestas. Phasellus interdum odio at sapien fringilla scelerisque. Mauris sagittis eleifend sapien, sit amet laoreet felis mollis quis. Pellentesque dui ante, finibus eget blandit sit amet, tincidunt eu neque. Vivamus rutrum dapibus ligula, ut imperdiet lectus tincidunt ac. Pellentesque ac lorem sed diam egestas lobortis.

Suspendisse leo purus, efficitur mattis urna a, maximus molestie nisl. Aenean porta semper tortor a vestibulum. Suspendisse viverra facilisis lorem, non pretium erat lacinia a. Vestibulum tempus, quam vitae placerat porta, magna risus euismod purus, in viverra lorem dui at metus. Sed ac sollicitudin nunc. In maximus ipsum nunc, placerat maximus tortor gravida varius. Suspendisse pretium, lorem at porttitor rhoncus, nulla urna condimentum tortor, sed suscipit nisi metus ac risus.

Aenean sit amet enim quis lorem tristique commodo vitae ut lorem. Duis vel tincidunt lacus. Sed massa velit, lacinia sed posuere vitae, malesuada vel ante. Praesent a rhoncus leo. Etiam sed rutrum enim. Pellentesque lobortis elementum augue, at suscipit justo malesuada at. Lorem ipsum dolor sit amet, consectetur adipiscing elit. Praesent rhoncus convallis ex. Etiam commodo nunc ex, non consequat diam consectetur ut. Pellentesque vitae est nec enim interdum dapibus. Donec dapibus purus ipsum, eget tincidunt ex gravida eget. Donec luctus nisi eu fringilla mollis. Donec eget lobortis diam.

Suspendisse finibus placerat dolor. Etiam ornare elementum ex ut vehicula. Donec accumsan mattis erat. Quisque cursus fringilla diam, eget placerat neque bibendum eu. Ut faucibus dui vitae dolor porta, at elementum ipsum semper. Sed ultrices dui non arcu pellentesque placerat. Etiam posuere malesuada turpis, nec malesuada tellus malesuada.

Contents

List of Figures

A List of Symbols and Abbreviations

e	Absolute charge of an electron $= 1.602 \times 10^{-19}\,\mathrm{C}$
ϵ_0	Permittivity of free space $= 8.854 \times 10^{-12}\,\mathrm{F\,m^{-1}}$
λ_D	Debye length $\equiv \sqrt{\frac{\epsilon_0 K T_e}{n_e e^2}}$
n_e	Plasma electron number density as a function of position
n_i	Plasma ion number density as a function of position
T_e	Plasma electron temperature
Z	Ion charge state in units of e
1D, 2D, 3D . .	One-, two- or three-dimension(al)
Otter	One of the finest of water mammals.
Hedgehog . . .	Quite a nice prickly friend.

Neque porro quisquam est qui dolorem ipsum quia dolor sit amet, consectetur, adipisci velit...

There is no one who loves pain itself, who seeks after it and wants to have it, simply because it is pain...

— Cicero's *de Finibus Bonorum et Malorum*

1 Introduction

Contents

1.1 A plan

Actually the very first thing to say will be the stuff about light i think, about diagnostic tools essentially always being about controlling the various properties of light (ie electromagnetic waves)

sections to include start with the laser and our entrance into the multi-petawatt regime with no signs of stopping - ref 40 in alex savin thesis - it looks like that is saying huge growth in laser power check that and maybe write in thesis but don't include the figure. Also include description of CPA and OPCPA what is a plasma modelling plasma with PIC codes intense lasers and absorption mechanisms?? yes for sure but dont do all just those just below ZVP simulation units and similarity parameter Frames of reference - lab, sim, ablating front sruface of plasma

what is the story? Based on first section by Alex after the abstract Plasma is ubiquitous in our known universe and plasma provides us huge opportunities as a tool to improve our lives (From chen) what we can see in the sky is a result of that stuff being in the plasma state. Lasers can do so much now and are only getting more powerful all the time thanks to CPA and since developments (discuss) Simulataneously our ability to understand the physics has been aided by an explosion in computing power (peter HEDP paper) In this thesis we discuss some of the opportunities that relativistic laser plasma physics offers us with solid density targets - note that note about solids v gases at this point. Perhaps even before the debye length, define what we mean by the temperature of the plasma??

An unused statement about ion immobility Assume for now that the ion-electron mass ratio is infinite, that is to say the ions are approximately immobile for the timescales under consideration, generally true for a fair few relativistic laser pulse cycles (In later sections the mobility of plasma ions will prove very important but for now this is ignored.).

1.2 The definition of a plasma

As outlined in F. Chen's definitive textbook 'Introduction to Plasma Physics and Controlled Fusion' [**chen20116**], a plasma must fulfil three criteria, namely,

1. Ionisation: a plasma must consist of both charged and neutral particles, of course this alone cannot define a plasma, any gas will contain some degree of ionisation;

2. Quasineutrality: while locally there can be (often extreme) electromagnetic forces and charge concentrations at work, over the length scales of the plasma,

such forces are screened out and the plasma bulk remains net neutral in charge;

3. Collective behaviour: unlike in a gas where collisions dominate, the particles in a plasma generate electromagnetic fields that interact at a distance and thus a particle's motion depends not only on its immediate viscinity but on the surrounding plasma conditions, indeed often it is the so-called 'collisionless' plasmas where collisions can be safely neglected that are of most interest, as is the focus of this thesis.

1.2.1 The Debye length

The Debye length describes the extent to which a plasma can shield electromagnetic fields within and so remain quasineutral. Consider an infinitely extending plasma with a test charge placed at some point, then what would be the potential $\phi(\mathbf{x})$? If the plasma had no kinetic energy, the charged particles would arrange themself immediately ajacent to the test charge and once this equilibrium state was reached there would be no electromagnetic fields present. Realistically the plasma will have some temperature, likely a very large temperature and so some particles will be able to escape the potential of the test charge and thus leak electromagnetic fields into the plasma bulk. Poisson's equation reads

$$\epsilon_0 \nabla^2 \phi = -e(Zn_i - n_e), \tag{1.1}$$

where $\epsilon_0 = 8.854 \times 10^{-12}\,\mathrm{F\,m^{-1}}$ is the permittivity of free space, $e = 1.602 \times 10^{-19}\,\mathrm{C}$ is the charge of an electron, Z is the plasma ion charge in units of e and n_i and n_e are the number densities of plasma ions and electrons.

Since the electrons are significantly more mobile than the ions due to their lower mass, it is in general the electrons and not the ions that respond to the test charge and the ions can be assumed to provide a constant background of positive charge density. If the number density of electrons follows a Boltzmann temperature distribution in the presence of a potential energy $-e\phi$, then

$$n_e = n_{e,0} e^{e\phi/KT_e}, \tag{1.2}$$

where $n_{e,0}$ is the electron number density far from the test charge, $n_i = n_{e,0}/Z$ and KT_e is the electron temperature. Note that in plasmas it is very common for different species to have differing temperatures depending on the mechanism for energy absorption and the timescales for collisions compared to the timescale of the study.

Substituting equation 1.2 into equation 1.1 and Taylor expanding the exponential term in the limit that the plasma is weakly coupled ($e\phi << KT_e$), obtains

$$\nabla^2\phi = \frac{\phi}{\lambda_D^2}, \tag{1.3}$$

where

$$\lambda_D \equiv \sqrt{\frac{\epsilon_0 KT_e}{n_e e^2}}, \tag{1.4}$$

is the *Debye length* and describes the thickness of the charge sheath surrounding the test charge. For quasineutrality to hold for the plasma bulk, its spatial dimensions must extend beyond a few Debye lengths.

1.2.2 The plasma parameter

In order for the above description to be statistically valid, there must be a large number of charged particles within the shielding sheath. The number of particles within the Debye sphere can be computed as

$$N_D = \frac{4}{3}\pi\lambda_D^3 n. \tag{1.5}$$

Note that, as discussed above, in most cases it is most suitable to choose the number density n to be the number density of electrons. To ensure the plasma is suitably ionised (criterion 1) and that the plasma engages in collective behaviour (criterion 3),

$$N_D >>> 1. \tag{1.6}$$

1.2.3 Collisionality and the plasma frequency

Collective behaviour not only depends on the ability for large numbers of particles to interact via electromagnetic forces but that these forces dominate over collisions in describing particle trajectories. Taking ω as the typical frequency of plasma

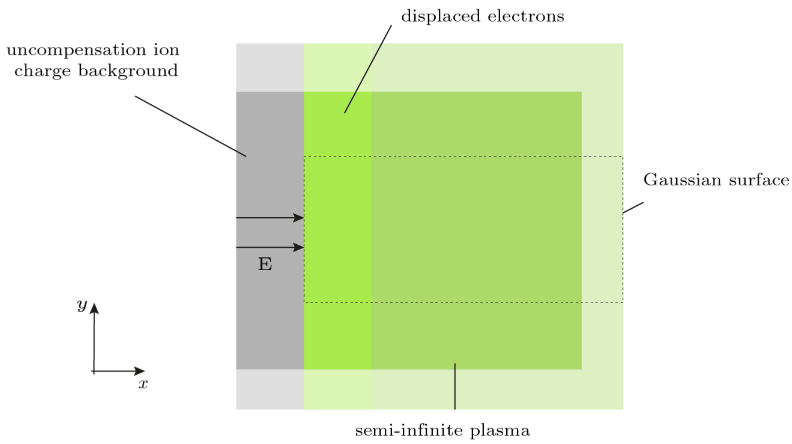

Figure 1.1: Diagram to illustrate the plasma frequency derivation.THIS FIGURE NEEDS E POINTING THE OTHER WAY

oscillations and τ as the average time between collisions, for a plasma (as opposed to a gas) must satisfy

$$\omega\tau > 1. \tag{1.7}$$

It now remains to determine what is the typical frequency of collisions in a given plasma. While the types of plasma waves and their associated frequencies of oscillation are multitudinous, the characteristic frequency, the *plasma frequency*, ω_p, is the most straightforward. It describes the response of electrons to charge imbalances within an infinite uniform plasma at rest in the absence of magnetic fields or temperature fluctuations. As noted in section 1.2.1, the ions provide a constant backgorund of positive charge.

Consider an semi-infinite plasma existing for $x > 0$, with electron density n_e and ion density n_e/Z of charge state Z[1]. Suppose the electron fluid is displaced by some perfectly isotropic force into the plasma bulk a distance $(\Delta x)\hat{\mathbf{x}}$ as in figure 1.1. The total charge of displaced electrons within a surface area of σ is

$$Q = -en_{\mathrm{e}}\sigma\Delta x. \tag{1.8}$$

[1]This description has direct relevance to the Zero Vector Potential mechanism which will be made clear later.

Applying Gauss' law to the surface detailed in figure 1.1, the uncompensated charge leads to

$$-\sigma E\hat{\mathbf{x}} = \frac{Q}{\epsilon_0}\hat{\mathbf{x}} = -\frac{en_e\sigma\Delta x}{\epsilon_0}\hat{\mathbf{x}} \tag{1.9}$$

at the electron surface. By the Lorentz force, the displaced electrons will experience a restoring force, $-eE\hat{\mathbf{x}}$, perpendicular to the surface due to the electron-ion charge imbalance. The equation of motion for electrons on that surface is therefore

$$m_e\frac{\mathrm{d}^2\Delta x}{\mathrm{d}t^2} = -eE = -\frac{e^2n_e}{\epsilon_0}\Delta x. \tag{1.10}$$

Equation 1.10 clearly describes a simple harmonic oscillator with a characteristic frequency given by the plasma frequency,

$$\omega_p = \sqrt{\frac{e^2n_e}{m_e\epsilon_0}}. \tag{1.11}$$

1.3 The Lawson-Woodward theorem

The Lawson-Woodward theorem states that there can be no net electron energy gain using laser fields [**esarey__2009__PhysicsLaserdrivenPlasmabaseda**], quite at odds with one of the primary aims of this thesis, that is, the acceleration of electrons. There are, however, several conditions that must be met, namely,

1. The interaction region is infinite;
2. The interaction occurs in a vacuum;
3. The electron is ultra-relativistic ($v \approx c$) along the acceleration gradient;
4. No electro- or magnetostatic fields are present;
5. Non-linear effects are neglected.

Several of these will be applicable to the various accelerations of electrons considered. It is this final condition that is most damning, throughout this thesis the ultra-relativistic laser pulses under consideration ensure non-linear effects cannot be neglected. It is indeed such non-linearities that are of interest.

1.4 Relativistic effects

The descriptor 'Relativistic' is applied liberally in this thesis. When applied to electromagnetic fields or laser pulses it refers to

$$a_0 \gg 1. \tag{1.12}$$

When applied to particles, their speeds are

$$v \approx c. \tag{1.13}$$

A relativistic laser pulse will accelerate electrons to relativistic velocities in a fraciton of a laser pulse cycle. Consider an electron in the presence of a uniform electric field of magnitude $a_0 = 100$, an intensity accessible by current state of the art laser facilities. The work done on that particle by the field is

$$U = (\gamma - 1)m_\mathrm{e}c^2 = \int \mathbf{E} \cdot \mathrm{d}\mathbf{x}, \tag{1.14}$$

where

$$\gamma = \frac{1}{\sqrt{1-\beta^2}}. \tag{1.15}$$

The field will accelerate an electron to a $\beta = 0.99$, corresponding to $\gamma \approx 7$, in less than 1 % of a corresponding laser pulse wavelength.

1.4.1 Conservation of generalised transverse momentum

Consider a holonomic system of N relativistic particles under the influence of electromagnetic forces. A particle j with charge e_j and mass m_j experiences a scalar potential,

$$U_j = e_j(\Phi - \mathbf{A} \cdot \mathbf{v}_j) \tag{1.16}$$

and hence the system is described by the Lagrangian

$$L = \sum_{j=1}^{N} \left(-m_\mathrm{j}c^2\sqrt{1-\beta_\mathrm{j}^2} - e_j(\Phi - \mathbf{A} \cdot \mathbf{v}_\mathrm{j}) \right), \tag{1.17}$$

where $\beta_j^2 = \mathbf{v}_\mathrm{j} \cdot \mathbf{v}_\mathrm{j}/c^2$ and $\mathbf{v}_j = \mathrm{d}\mathbf{x}_j/\mathrm{d}t$ [1]. The generalised momentum corresponding to coordinate x_j is

$$p_{j,x} = \frac{\partial L}{\partial \dot{x}_j} = m_j \dot{x}_j + e_j A_x, \tag{1.18}$$

thus, the generalised momentum describes both the linear mechanical momentum and the momentum of the electromagnetic field. Via Noether's theorem, if L is independent of x_j, *i.e.* spatially homogeneous along x for particle j, then

$$\dot{p}_{j,x} = 0 \tag{1.19}$$

since

$$\frac{\mathrm{d}}{\mathrm{d}t}\left(\frac{\partial L}{\partial \dot{x}_j}\right) = \frac{\partial L}{\partial x_j}. \tag{1.20}$$

Consider a linearly polarised Gaussian laser pulse, with axis of polarisation along x incident on a solid target at rest. Then A_x is approximately constant along x near the beam centre[2]. Integrating equation 1.21 and noting that initially there is no linear or electromagnetic momentum at the target, the generalised transverse momentum conservation equation for an electron in the laser field is

$$p_\mathrm{T} = eA, \tag{1.21}$$

where p_T is the electron momentum along the polarisation axis of the laser pulse and A it the laser pulse vector potential.

Note that this is only valid provided the electron does not radiate along the direction of polarisation as discussed by Sokolov *et al* [2]. The implications of 'Radiation Reaction' are discussed in the following section.

1.5 QED effects

We are now at the cusp of **SF-QED!** (**SF-QED!**) laser-plasma physics. Access to this regime will enable the testing of decades old theoretical predictions. Already Fedeli *et al* have shown in simulations that current PW-class laser facilities can

[2]**Constant relative to the scale of typical electron trajectories in such an interaction.**.

access the regime using an all-optical set up based on laser-solid surface interactions [**fedeli_2020_ProbingStrongfieldQED**]. The primary two SF-QED phenomena to be accessed are Radiation Reaction and multi-photon Breit-Wheeler electron pair production. Brief introductions to these phenomena are now presented.

1.5.1 High-energy photon emission and radiation reaction

When a charged particle undergoes an acceleration, it emits electromagnetic radiation. If the electromagnetic field is sufficiently strong, *i.e.* approaching the Schwinger Limit in the rest frame of the particle, then a non-neglible fraction of particle momentum can be transferred to the emitted high energy photon via inverse Compton scattering, substantially impacting the dynamics of the accelerated particle. This back reaction is known as Radiation Reaction.

Note for in simulation section: 'The processes discussed in this section bring into play a characteristic length [the classical radius of the electron

in classical electrodynamics (CED) or the standard Compton wavelength

in quantum electrodynamics (QED)]. As a result, a simulation will require the user to define the absolute scale of the system by defining the referencangularfrequencySI parameter' ' Also there are a list of assumptions in smilei that I should state in the simulation section and demonstrate they are all fine.

1.5.2 Multi-photon Breit-Wheeler pair production

(This has been written up from smilei but should probs get reference elsewhere??) > check out savin thesis

Multi-photon Breit-Wheeler pair production, also known as non-linear Breit-Wheeler is the decay of a high energy photon, typically produced via **RR!** (**RR!**), into an electron-positron pair in the presence of a strong electromagnetic field, explicitely,

$$\gamma + n\omega \rightarrow e^- + e^+. \tag{1.22}$$

The strength of the effect is dependent on the lorentz invariant photon quantum parameter,

$$\chi_\gamma = \frac{\gamma_\gamma}{E_\mathrm{s}}\sqrt{(\mathbf{E}_\perp + \mathbf{c}\times\mathbf{B}^2},\tag{1.23}$$

where $E_\mathrm{s} = 1.3\times10^{18}\,\mathrm{V\,m^{-1}}$ is the Schwinger electric field, $\gamma_\gamma = \epsilon_\gamma/m_\mathrm{e}c^2$, the normalised photon energy and $\mathbf{E}_\perp$ the electric field perpendicular to the photon propagation direction. Cite Smilei and say, in a constant E-field, the rate of pair production increases rapidly up to $\chi_\gamma \approx 10$ at which point it saturates and slowly reduces.

If the electron radiates all its energy to the photon, for the ZVP mechanism, at the point of emission one finds,

$$\chi_\gamma = |\mathbf{E}|\frac{1+\frac{a_0^2}{\bar{n}_\mathrm{e}}}{E_\mathrm{s}}\sqrt{2},\tag{1.24}$$

The chi parameter will change rapidly once the transition to QED ZVP has occured due to the change in scaling.

1.6 Simulations

1.6.1 Particle-In-Cell codes

Other considerations:(At some point list all the other sources of potential error, including ignoring ionisation, ionisation states, collisions.) I think put this in the main intro section. Then start PIC codes with discretisation of the Vlasov-Maxwell system of equations.

The Vlasov-Maxwell system of equations

A collisionless and fully ionised plasma is fully described in the kinetic description by the Vlasov-Maxwell system of equations [3]. Each plasma species, s, of particles with mass m_s and charge q_s is described by its distribution function $f_s(t,\mathbf{x},\mathbf{p})$ at time t, position $\mathbf{x}$ and momentum $\mathbf{p}$. The distribution satisfies the Vlasov equation, that is,

$$(\partial_t + \frac{\mathbf{p}}{m_s\gamma}\cdot\nabla + \mathbf{F}_\mathrm{L}\cdot\nabla_\mathbf{p})f_s = 0,\tag{1.25}$$

where $\gamma = \sqrt{1 + \mathbf{p}^2/(m_s c)^2}$ is the relativistic Lorentz or gamma factor of the distribution and

$$\mathbf{F}_{\mathrm{L}} = q_s(\mathbf{E} + \mathbf{v} \times \mathbf{B}) \tag{1.26}$$

is the Lorentz force that acts on a particle with velocity $\mathbf{v} = \mathbf{p}/m_s\gamma$. The electric $\mathbf{E}(t, \mathbf{x})$ and magnetic $\mathbf{B}(t, \mathbf{x})$ fields that create the force must satisfy Maxwell's equations,

$$\nabla \cdot \mathbf{B} = 0, \tag{1.27}$$

$$\nabla \cdot \mathbf{E} = \frac{\rho}{\epsilon_0}, \tag{1.28}$$

$$\nabla \times \mathbf{B} = \mu_0 \mathbf{J} + \mu_0 \epsilon_0 \partial_t \mathbf{E}, \tag{1.29}$$

$$\nabla \times \mathbf{E} = -\partial_t \mathbf{B}. \tag{1.30}$$

Here ϵ_0 and μ_0 are the vacuum permittivity and permeability respectively.

This self-consistent system of equations describes the dynamics of plasma particles within electromagnetic fields. The particles then modify the fields via their charge and current densities,

$$\rho(t, \mathbf{x}) = \sum_s q_s \int d^3p f_s(t, \mathbf{x}, \mathbf{p}), \tag{1.31}$$

and

$$\mathbf{J}(t, \mathbf{x}) = \sum_s q_s \int d^3p \mathbf{v} f_s(t, \mathbf{x}, \mathbf{p}), \tag{1.32}$$

respectively.

Discretisation of the Vlasov-Maxwell equations

Finding numerical solutions to the Vlasov-Maxwell equations is no straightforward task, there are codes that are capable such as Valis **CITE**, however, the requirement of high resolution in both position and momentum is exceedingly costly and use of such codes are limited in their size, duration and spatial dimensions. A

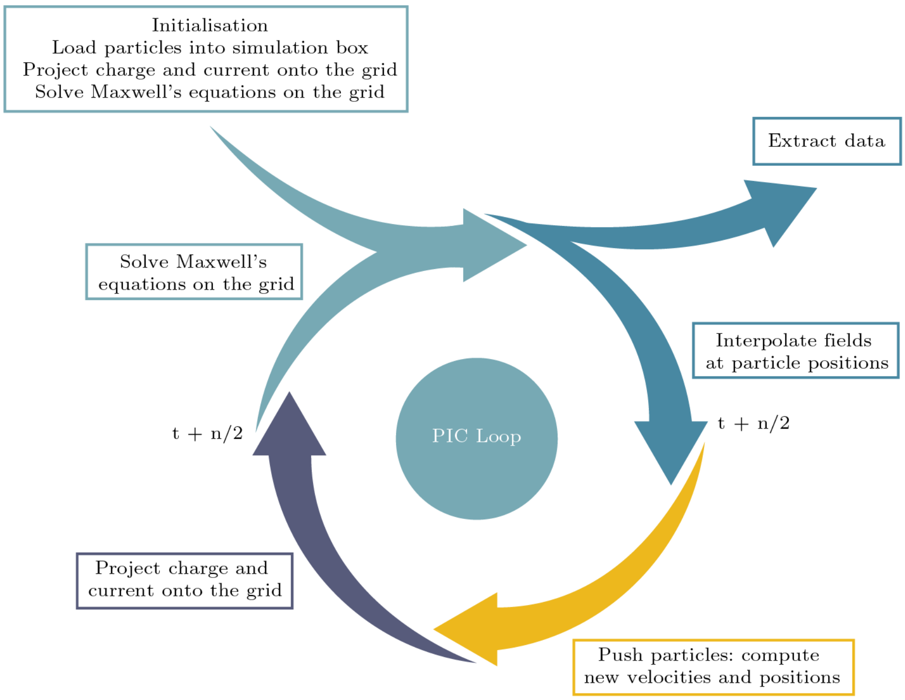

Figure 1.2: Diagram of the PIC code algorithm

more tractable approach is to discretise the distribution function into N_s 'quasi-particles'[3] (often referred to as 'macro-particles' in practice, typically representing a large number of real particles), such that

$$f_s(t, \mathbf{x}, \mathbf{p}) = \sum_{p=1}^{N_s} w_p S(\mathbf{x} - \mathbf{x}_p(t)) \delta(\mathbf{p} - \mathbf{p}_p(t)), \tag{1.33}$$

where w_p is the quasi-particle's weight, $\mathbf{x}_p$ and $\mathbf{p}_p$ are its position and momentum respectively, δ is the Dirac-delta distribution and $S(\mathbf{x})$ the shape-function chosen to represent the quasi-particle. The Vlasov equation is then integrated along the continuous trajectories of the quasi-particles while Maxwell's equations are solved on a discrete spatial grid of 'cells'. Such a code is aptly named a 'PIC' code. A schematic of the PIC code algorithm is presented in figure 1.2. After initialising particles, Maxwell's equations are solved with the Finite Difference Time Domain (FDTD) ap-

[3] Originally introduced by Langdon and Birdsall as 'clouds' [**langdonTheoryPlasmaSimulation1970**].

proach [**tafloveComputationalElectromagneticsFiniteDifference2005**] where electromagnetic fields are discretised the staggered 'Yee grid'. This ensures

HMM Im confused... read langdon maybe and redo this section then?

To ensure space and time centering of the electromagnetic field derivatives in Maxwell's equations, electric and magnetic fields are discretised on the staggered 'Yee grid'. Electric fields are defined at integer time steps, n while magnetic fields at half-integeter $(n + 1/2)$ time steps. Note, for the particle pusher it is also required that the magnetic fields also be defined at integer steps. Particles are advanced in time using a 'leap-frog' scheme, where positions are defined at integer timesteps and momenta at half integer.

Using a momentum and charge conserving scheme (cite Esekipov sheme for charge conservation used by Smilei.).

Well known Boris pusher

Smilei

Smilei (for Simulating Matter Irradiated by Light at Extreme Intensities) is a modern collaborative, massively-parallel, fully relativistic and open source plasma physics PIC code and was the main workhorse for this thesis[4]. Produced by M. Grech's team(CHECK THIS) at École Polytechnique [3], its development was motivated by the rapid development of multi-petawatt facilities globally including their local Apollon laser and by supercomputing power which has 'skyrocketed' in recent years [3]. Indeed, the work in this thesis with 3D simulations required over 1×10^6 cores.

Reference quantities

This needs rewording so as not to be the same as paper.

Reference units

To great convenience, Smilei operates in normalised units. This normalisation is not chosen *a priori*, instead results can be scaled by an arbitrary reference angular frequency. This is extremely useful when working with boosted frames of reference.

[4] At points benchmarks agaist the EPOCH and Osiris PIC codes were performed.

Units of	SI units	Normalisation
velocity	$\mathrm{m\,s^{-1}}$	c
charge	C	e
mass	kg	m_e
momentum	$\mathrm{kg\,m\,s^{-1}}$	$m_\mathrm{e}c$
energy/temperature	J	$m_\mathrm{e}c^2$
time	s	ω_L^{-1}
length	m	c/ω_L
number density	$\mathrm{m^{-3}}$	n_c
electric field	$\mathrm{V\,m^{-1}}$	$m_\mathrm{e}c\omega_\mathrm{L}/e$

Table 1.1: Smilei normalisations for common quantities with the laser angular frequency ω_L set at the reference angular frequency.

As this thesis focuses on the interaction of a laser pulse with plasma, the laser pulse angular frequency, ω_L is set as the frequency of reference. A list of the most common normalisations are given in table 1.1.

General simulation parameters

Boundary conditions "Silver-Müller" boundary conditions for the simulation box edges **cite - H Barucq Asymptomatic analysis 1997**. These are able to absorp and inject electromagnetic waves and particles. Note that there can be non-physical reflection of electromagnetic waves at such boundaries leading to error.

Shape function The quasi-particle shape function $S(\mathbf{x})$ describes how to project charge onto the grid. It is symmetric in all dimensions with respect to $\mathbf{x}$ and extends over n cells of width Δx in each direction where n is the interpolation order. It can be written as a product across D dimensions,

$$S(\mathbf{x}) = \Pi_{\mu=1}^{D} s^{(n)}(x^\mu). \tag{1.34}$$

Smilei implements orders 2, 3 and 4, the explicit shape functions are

$$s^2(n) = \begin{cases} \frac{1}{\Delta x}\left(1 - \left|\frac{x}{\Delta x}\right|\right) & \text{if } |x| \leq \Delta x, \\ 0 & \text{otherwise,} \end{cases} \tag{1.35a}$$

$$s^3(n) = \begin{cases} \frac{3}{4\Delta x}\left(1 - \frac{4}{3}\left(\frac{x}{\Delta x}\right)^2\right) & \text{if } |x| \leq \frac{1}{2}\Delta x, \\ \frac{9}{8\Delta x}\left(1 - \frac{2}{3}\left|\frac{x}{\Delta x}\right|\right)^2 & \text{if } \frac{1}{2}\Delta x < |x| \leq \frac{3}{2}\Delta x, \\ 0 & \text{otherwise,} \end{cases} \tag{1.35b}$$

$$s^4(n) = \begin{cases} \frac{2}{3\Delta x}\left(1 - \frac{3}{2}\left(\frac{x}{\Delta x}\right)^2 + \frac{3}{4}\left|\frac{x}{\Delta x}\right|^3\right) & \text{if } |x| \leq \Delta x, \\ \frac{4}{3\Delta x}\left(1 - \frac{1}{2}\left|\frac{x}{\Delta x}\right|^3\right) & \text{if } \Delta x < |x| \leq 2\Delta x, \\ 0 & \text{otherwise.} \end{cases} \tag{1.35c}$$

Parallelisation

Modern **HPC!** (**HPC!**) systems are poised to enter the exascale regime ($> 10^{18}$ Floating Point Operations Per Second). With limited improvements in microprocessor technoligies, such power is acheived through massive parallelisation across processing units. To enable the study of the dynamics of up to billions of macroparticles, PIC codes test the limits of current supercomputing architectures.

Supercomputing resources

ARCHER2, the UK's national supercomputer came online in November 2021, with it delivering over ten times the reseources of its predecessor (ARCHER) [4]. An HPE Cray EX supercomputing system with a peak performance estimated at 28 Pflops s^{-1} across 5860 nodes each with dual AMD EPYCTM 7742 64-core processor for a total of 750,080 cores, ARCHER2 was able to supply the resources required to run the costly PIC simulations for this research. The substantially cheaper HYADES simulations were performed using the Rutherford Appleton Laboratory's SCARF **HPC!** cluster [**SCARFOverview**].

2 The Zero Vector Potential Absorption Mechanism

Contents

2.1 Motivations and an overview

****This is from paper cover letter and acts as an abstract for this chapter, I also need to go through and add citations****

Throughout the history of experimental science, light has been the primary tool for investigation. Through the creation of synchrotron radiation sources and more recently XFELs, electron bunches have been used to create increasingly specialised light sources for the study of matter of all kinds. At Diamond Light Source in the UK, electron beams have been used for a diverse range of studies from new drugs to ancient paintings, while at SLAC, the United States' forefront electron accelerator, common applications hail from many disciplines: science, medicine, industry and homeland security. Hence, much research has been done to produce electron bunches with ever greater charge, energy and coherency. Multi-petawatt laser facilities are now available across the globe for the study of laser-plasma interactions at ever greater peak intensities. In the ultra-relativistic regime $a_0 \gg 1$, there is a novel method for high-charge electron bunch creation. Via relativistic effects, a laser pulse organises the electrons at the surface of a solid density plasma into coherent bunches, which are then ejected at high speeds. Those discussed in this thesis have properties rivalling those of forefront accelerators. The quality, charge and duration of the attosecond electron bunches described here would enable the study of the most fundamental interactions of our universe. While there has been some experimental evidence for attosecond electron bunches from intense laser-solid interactions, here is proposed a new mass-limited target setup to generate electron bunches with greater charge density. Such electron bunches are fully characterised using PIC simulations to compare their quality to those of existing electron bunch production methods and their energies described via the Zero Vector Potential Mechanism. Their implications for laser to plasma energy absorption are also considered including at the onset of **SF-QED!** effects.

These results have excited the community to perform experiments to realise these electron bunches for the creation of ultra-bright X-ray pulses: having recently completed an experimental campaign at the ORION laser facility, studying high harmonic generation from such electron bunches, the author's proposal has been accepted to observe the electron bunches directly at the GEMINI PW laser at the Central Laser Facility, UK.

This chapter is organised as follows.

****I must add the chapter outline here****

2.2 Introduction

Of primary interest in this thesis is the interaction of a relativistically intense short-pulse laser interacting with a solid density plasma target with a sharp density gradient. Now is presented an explanation of this interaction: the ZVP mechanism of attosecond absorption of laser pulse energy, proposed by *Baeva et al* [5] and later developed by *Savin et al* [6, 7]. Laser energy absorption in dense plasmas was first proposed by Wilks and Kruer [8], via a ponderomotive mechanism where plasma electrons are heated directly by the laser pulse via the so-called $\mathbf{J} \times \mathbf{B}$ force.

This thesis is interested in the 'post-ponderomotive' regime where the frequency of the relativistic plasma oscillations ($\omega_{\mathrm{p}} \sim \sqrt{S}$) are greater than the $\mathbf{J} \times \mathbf{B}$ induced plasma electron oscillations at $2\omega_{\mathrm{L}}$. The plasma electrons' response is then fast enough to compensate the ponderomotive pressure of the laser pulse with the formation of electrostatic fields between electrons and ions and so respond adiabatically to the applied $\mathbf{J} \times \mathbf{B}$ force. Hence, plasma electrons cannot be heated directly by the laser pulse. Interestingly, working through this condition suggests the criterion for the ZVP regime is $S > 4$, slightly more constraining than $S > 1$ as is typically stated for the ZVP regime [7]. The resolution comes from understanding the plasma response. The bulk plasma must have $S > 1$ to prevent relativistic transparency and so ensure a laser-surface interaction. Then the ponderomotive pressure of the laser is able to compress the front surface to densities such that the overdensity condition is satisfied. Note that to neglect the pre-adiabatic formation phase requires a sufficiently steep density gradient around the relativistic critical density surface (where $S = 1$) to shift the main interaction to a region where this condition on the overdensity is satisfied. Pre-plasma formation and scale length will be discussed in great detail in a later chapter.

Provided all conditions are met, the ponderomotive pressure of the laser compresses the electrons at the front surface of the plasma and so shifts the laser-plasma surface interaction to plasma densities well beyond the relativistic critical density, leaving in its wake a positive space charge. This electron-ion charge separation leads to the formation of a *pseudo-capacitor* electrostatic field. So

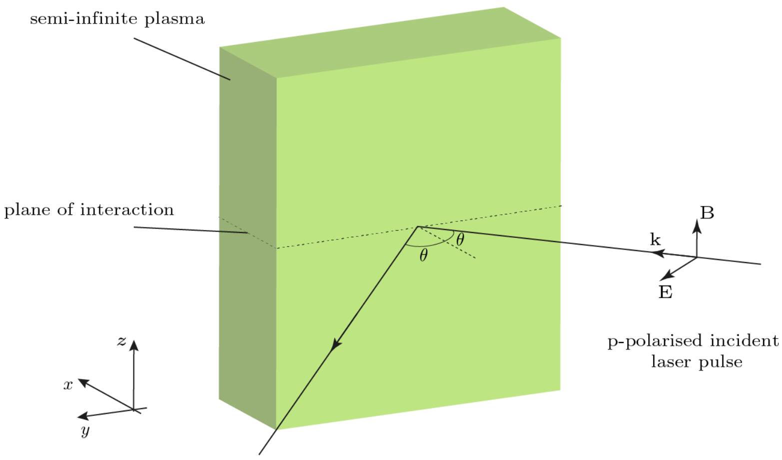

Figure 2.1: Diagram of a p-polarised laser pulse incident at angle θ specularly reflected from a solid density plasma. By considering the Lorentz force equation, it is clear that all forces and therefore all plasma particle dynamics are confined to a plane.

we have entered a regime of adiabaticity where the plasma skin layer is confined within a potential well consisting of the ponderomotive pressure and the Coulomb potential of the pseudocapacitor field. Thus is formed a high density and spatially thin electron bunch (sometimes referred to as an electron sheath in the literature [9]) at the plasma surface.

To understand this system, consider now a relativistic linearly polarised laser pulse obliquely incident, at an angle of incidence θ, on a semi-infinite plasma, existing for $x \geq 0$ as in figure 2.1. The Hamiltonian of a single electron confined within the potential well [1] is

$$\mathcal{H} = c\sqrt{m_{\mathrm{e}}^2 c^2 + |\mathbf{p}|^2} - e\Phi. \tag{2.1}$$

Here, the second term of equation 2.1 describes the contribution to the electron's energy from the electrostatic potential, Φ, of the pseudo-capacitor. The first term is the electron energy, U, extracted from the invariant of the relativistic 4-momentum of the electron, $\mathbf{P}^\mu = (U/c, \mathbf{p})$,

$$\mathbf{P}^\mu \cdot \mathbf{P}_\mu = \frac{U^2}{c^2} - |\mathbf{p}|^2 = m_{\mathrm{e}}^2 c^2. \tag{2.2}$$

Note that while there has been growing interest in the curvature of spacetime by relativistic lasers [**cite edward here**], for modern high power lasers, this effect remains undetectable. Thus, throughout this thesis the inner product of 4-vectors is defined using the Minkowski Metric [10].

Decomposing the electron's 3-momentum into orthogonal components: p_{prop}, along the laser propagation direction, p_{pol}, along the polarisation axis of the laser pulse and $p_{\perp}$, perpendicular to both, there are two simplifications to be made. Firstly, by canonical conservation of transverse momentum, $p_{\text{pol}} = eA$, where A is the laser vector potential amplitude. Secondly, in the case of a p-polarised laser pulse (the known optimum for ZVP electron bunch generation [6] and High Harmonic Generation (HHG) [11]), with reference to figure 2.1 and the Lorentz force law, the forces at play confine the electron trajectory to the p_{prop}-p_{pol} plane and the essential interaction geometry is two-dimensional. This is provided one considers length scales smaller than the focal spot of the laser pulse on the target such that the pondermotive pressure is normal to the target surface.

Explicitly, the Hamiltonian can be written as

$$\mathcal{H} = c\sqrt{m_e^2c^2 + p_{\text{prop}}^2 + e^2A^2} - e\Phi. \tag{2.3}$$

From equation 2.3 it is clear that should the vector potential pass through zero, one of the walls of the potential well is totally suppressed, allowing electrons in the skin layer to escape the plasma, breaking adiabaticity. The necessity of vector potential zeros for this violent reconstruction of the plasma surface led Baeva *et al* [5] to coin the term 'Zero Vector Potential' mechanism to describe this process. Indeed, while elementary electromagnetism tells us a laser pulse will exponentially decay within a skin layer of a plasma without passing through zero, Baeva *et al* [5] were able to demonstrate in PIC simulations that for this regime, zeros do exist and do propagate through the skin layer. The explanation relies on a Doppler shift in the laser field due to the relativistic motion of the ablating plasma surface, and the mathematical formalism of this process proceeds as follows.

****Must also discuss the impact of relativity in creating the observed phenomena, probably at energy scaling section?****

As the ZVP mechanism is a relativistic phenomenon, it is essential to perform this analysis relativistically. Since all electrons are accelerated by the relativistic laser pulse to approximately speed c, surface electrons undergo similar trajectories and act collectively, oscillating in the laser pulse field. Consider first a transformation to the frame of reference where the laser pulse is normally incident to the plasma surface, this frame travels at velocity $\mathbf{v} = (c \sin\theta)\hat{\mathbf{y}}$ with electrons streaming at $-\mathbf{v}$. ****This needs adjusting for transverse momentum when there is an initial component that is non zero**** Using equation 2.2 and $U = \gamma m_\mathrm{e} c^2$,

$$\gamma^2 = 1 + a_0^2 + \left(\frac{p_\mathrm{prop}}{m_\mathrm{e} c}\right)^2, \tag{2.4}$$

where all parameters are in the boosted frame. Using $\mathbf{p} = \gamma m_\mathrm{e} \mathbf{v}$, the longitudinal velocity is

$$v_\mathrm{prop} = \frac{\tilde{p}_\mathrm{prop} c}{\sqrt{1 + a_0^2 + \tilde{p}_\mathrm{prop}^2}}, \tag{2.5}$$

where $\tilde{p}_\mathrm{prop} = p_\mathrm{prop}/m_\mathrm{e} c$. Thus, should the vector potential pass through zero, the surface is able to propagate towards the laser pulse at very close to speed c. Transforming back to the laboratory frame at the peak of ablation ($\mathbf{u} \approx -c\hat{\mathbf{x}}$) and using the equations for relativistic velocity addition,

$$\mathbf{u}'_\parallel = \frac{\mathbf{u} - \mathbf{v}}{1 - \mathbf{u}\cdot\mathbf{v}/c^2}, \tag{2.6}$$

$$\mathbf{u}'_\perp = \frac{\mathbf{u}_\perp}{\gamma_v (1 - \mathbf{u}\cdot\mathbf{v}/c^2)}, \tag{2.7}$$

where $\gamma_v = 1/\sqrt{1 - |\mathbf{v}|^2/c^2}$ [10], one finds that this peak ablation at speed $\approx c$ occurs now in the specular reflection direction. Simultaneity is broken and ripples co-move along the surface with the incident laser pulse wavefronts.

Transform now to the rest frame of the ablating front. Beyond the relativistic critical density surface, the vector potential of the laser pulse decays evanescently. At the spatial centre of the laser pulse, it can be described simply by

$$\mathbf{A}'_\mathrm{L}(t', r') = A'_0 \cos(\omega'_\mathrm{L} t') \exp(-r'/\delta') \hat{\mathbf{r}}'_\mathrm{pol} = A'_\mathrm{L} \hat{\mathbf{r}}'_\mathrm{pol}, \tag{2.8}$$

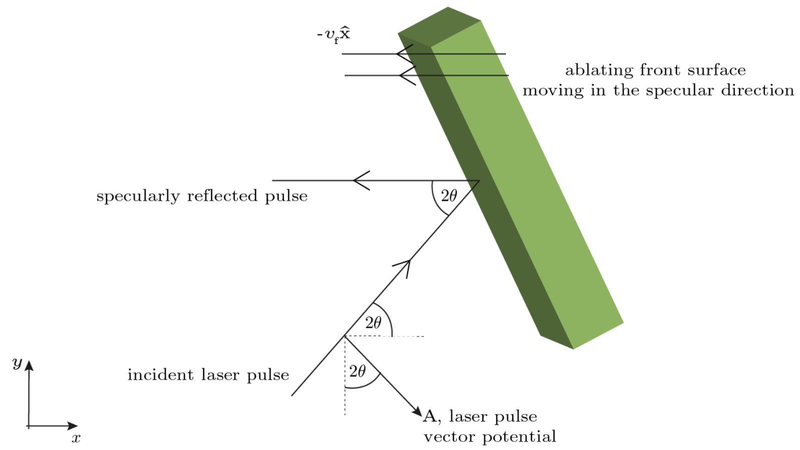

Figure 2.2: Diagram of a p-polarised laser pulse incident on an ablating overdense plasma. The laser is incident obliquely at an angle of θ and is reflected specularly. The plasma ablates specularly also. The interaction geometry is confined to a 2D plane.

where the primed symbols indicate that these quantities are measured in the rest frame of the expanding front, A'_0 is the vector potential amplitude and ω'_{L} is the frequency of the laser pulse, r' is the propagation distance of the laser into the plasma, δ' is the skin depth and $\hat{\mathbf{r}}'_{\mathrm{pol}}$ a unit vector defining the polarisation direction of the laser pulse. Un-primed coordinates will indicate the lab frame measurements.

****For sure include a diagram of lorentz boost and change of structure in ablating front, also PIC simulation of surface ripples?****

While previous demonstrations of the existance of vector potential zeros assumed that the ablation occurs normal to plasma surface, it is necessary to confirm that zeros are still predicted for specular ablation. Consider a p-polarised laser pulse confined to the x-y plane incident with an angle of incidence θ on an ablating overdense plasma expanding with velocity $-v_f\hat{\mathbf{x}}$ in the lab frame, as in figure 2.2. The direction of polarisation is

$$\hat{\mathbf{r}}_{\mathrm{pol}} = \hat{\mathbf{x}} \sin 2\theta - \hat{\mathbf{y}} \cos 2\theta \tag{2.9}$$

and the velocity of the rest frame of the ablating front relative to the lab frame is $-v_f\hat{\mathbf{x}}$.

****Include a section in the intro describing laser reflection off a plasma, including calculation of skin depth and once have calculated bunch thickness using oblique thing, determine skin depth etc****

Applying the Lorentz transformation to the electromagnetic 4-potential,

$$\mathbf{A}_\mu = (\phi/c, \mathbf{A}), \tag{2.10}$$

explicitly,

$$\mathbf{A}'_\mu = \Lambda^\mu_\nu \mathbf{A}_\nu, \tag{2.11}$$

where Λ^μ_ν, the Lorentz transform in this geometry is

$$\Lambda^\mu_\nu = \begin{pmatrix} \gamma & -\beta\gamma & 0 & 0 \\ -\beta\gamma & \gamma & 0 & 0 \\ 0 & 0 & 1 & 0 \\ 0 & 0 & 0 & 1 \end{pmatrix} \tag{2.12}$$

and here $\beta = -v_\mathrm{f}/c$, $\gamma = 1/\sqrt{1-\beta^2}$. Immediately from the y-coordinate transformation,

$$A'_\mathrm{L} \cos 2\theta' = A_\mathrm{L} \cos 2\theta. \tag{2.13}$$

Applying the headlight effect for a source moving at an angle 2θ to the boosted frame (a full derivation is given in Appendix A.1),

$$\cos(2\theta') = \frac{\cos(2\theta) - \beta}{1 - \beta\cos(2\theta)} \tag{2.14}$$

and rearranging equation 2.13, the vector potential in the lab frame is

$$A_\mathrm{L} = \frac{1 - \beta\sec(2\theta)}{1 - \beta\cos(2\theta)} A'_0 \cos(\omega'_L t') \exp(-r'/\delta'). \tag{2.15}$$

Writing the boosted frame space-time coordinates in terms of the lab frame coordinates,

$$ct' = \gamma(ct - \beta x), \tag{2.16}$$

$$x' = \gamma(x - \beta ct), \tag{2.17}$$

yields

$$A_\mathrm{L} = A_0 \cos(\omega_L t - kx) \exp\left(-\frac{\sqrt{(x-\beta ct)^2 + (y/\gamma)^2}}{\delta}\right), \tag{2.18}$$

where

$$A_0 = \frac{1 - \beta\sec(2\theta)}{1 - \beta\cos(2\theta)} A'_0, \tag{2.19}$$

$$\omega_L = \gamma\omega'_L, \tag{2.20}$$

$$k = \frac{\beta\gamma\omega'_L}{c}, \tag{2.21}$$

$$\delta = \frac{\delta'}{\gamma}. \tag{2.22}$$

The oscillatory term in equation 2.18 demonstrates the propagation of vector potential zeros within the plasma target. From the structure of this term it would appear that these zeros are expelled from the plasma along the specular direction at a speed

$$v_\phi = \frac{\omega_L}{k} = \frac{c}{\beta} = -\frac{c^2}{v_\mathrm{f}}. \tag{2.23}$$

****Could also discuss here about how relativistic similarity theory derives that zeros move at speed c but how that cannot be valid since then we would always have infinitely thin radiation pulses, unless there is an extended range of zero? I suppose there is some radiation happening around the peak? Good questions.. One remaining consideration is we require that the zero gets through the whole electron bunch which is generally at very high density but is also very thin, in a way is this skin depth not what precisely determines the bunch width? The bunch will be compressed until the skin depth goes to zero across it perhaps? Things to think about.****

To summarise, for a sufficiently intense laser pulse, electrons on the radiated surface of a solid target are accelerated by the laser to relativistic velocities at a fraction of a laser pulse cycle and therefore electrons both follow similar trajectories and are able to respond adiabatically to the $\mathbf{J} \times \mathbf{B}$ force of the laser pulse. They form into a high charge density spatially thin coherent electron bunch on the front surface of the plasma but displaced inwards from the approximately immobile ions via the ponderomotive pressure of the laser. This charge separation generates a longitudinal electrostatic pseudocapacitor field that confines electrons to a potential well on the front surface of the plasma, preventing further propagation of the electron bunch into the plasma bulk. When the zero of the vector potential passes through the electron bunch, the ponderomotive pressure instantaneously vanishes and electrons are ejected specularly from the target, copropagating with the zeroes and gaining energy as they discharge the pseudocapacitor field. The electron bunch is then rotated by the laser pulse and launched into the bulk at high energy, as it does so emitting coherent synchrotron radiation in transmission and reflection.

2.2.1 ZVP electron bunch energies

In [5], Baeva *et al* propose energy scalings for electron bunches produced in the ZVP regime as a function of the incident laser pulse intensity and plasma density, finding that one of the key statements of similarity theory ($p \sim a_0 S^x$, where x is some integer value, **THIS NEEDS A CITE I THINK IT APPEARS IN BAEVAS ORIGINAL HHG PAPER**) holds for the ZVP mechanism. Later this was then extended to three-dimensions (3D) by Savin *et al* [6]. What follows is that discussion with close consideration of both the consequences and constants of proportionality.

Consider again the semi-infinite block of plasma presented in figure 1.1, normally irradiated by a laser pulse with wavelength λ_{L} and peak electric field, E_{L}. It is now the ponderomotive pressure of the laser that displaces the electron fluid. The electron surface moves inwards until the pressure exerted by the peak instantaneous ponderomotive pressure of the laser pulse cycle,

$$\mathbf{P}_{\mathrm{L}} = \epsilon_0 E_{\mathrm{L}}^2 \hat{\mathbf{x}} = \epsilon_0 \left(\frac{a_0 \omega_{\mathrm{L}} m_{\mathrm{e}} c}{e} \right)^2 \hat{\mathbf{x}} \tag{2.24}$$

is equal and opposite to the pressure exerted by the pseudo-capacitor field,

$$\mathbf{P}_{\mathrm{C}} = \frac{QE}{\sigma} \hat{\mathbf{x}} = -\frac{(e n_{\mathrm{e}} \Delta x)^2}{\epsilon_0} \hat{\mathbf{x}} \tag{2.25}$$

from equations 1.8 and 1.9. Equating the magnitudes of $\mathbf{P}_{\mathrm{L}}$ and $\mathbf{P}_{\mathrm{C}}$, the maximum displacement inwards of electrons is

$$\Delta x \hat{\mathbf{x}} = \frac{c}{\omega_{\mathrm{L}}} \frac{a_0}{\bar{n}_{\mathrm{e}}} \hat{\mathbf{x}} = \frac{1}{kS} \hat{\mathbf{x}}, \tag{2.26}$$

where k is the wave-vector of the laser pulse. Correspondingly,

$$E = \frac{e n_{\mathrm{e}}}{\epsilon_0} \Delta x = \frac{\omega_{\mathrm{L}} c m_{\mathrm{e}} a_0}{e} = E_{\mathrm{L}}. \tag{2.27}$$

Applying the results of equations 2.26 and 2.27, when the ponderomotive pressure vanishes and the electron bunch is launched across the pseudo-capacitor, the relativistic kinetic energy gained by a single electron is

$$T = \int \mathbf{F} \cdot \mathrm{d}\mathbf{s} = \int_{\Delta x}^{0} -eEdx = \int_{\Delta x}^{0} -\frac{en_{\mathrm{e}}x}{\epsilon_0}dx = \frac{1}{2}m_{\mathrm{e}}c^2\frac{a_0^2}{\bar{n}_{\mathrm{e}}} \tag{2.28}$$

or an electron gamma factor,

$$\gamma = \frac{1}{\sqrt{1-\beta^2}} = 1 + \frac{a_0^2}{2\bar{n}_{\mathrm{e}}}. \tag{2.29}$$

Assuming all displaced electrons are captured by the potential well and launched as a coherent bunch, the total number of electrons in the bunch is

$$N_{\mathrm{e}} = n_{\mathrm{e}}\sigma\Delta x = \frac{\sigma a_0 n_{\mathrm{c}}}{k} = \sigma\epsilon_0 E_{\mathrm{L}} \tag{2.30}$$

and hence, the total kinetic energy of the electron bunch is

$$U_{\mathrm{ZVP}} = N_{\mathrm{e}}T = \frac{\sigma n_{\mathrm{c}}}{k} \times \frac{1}{2}m_{\mathrm{e}}c^2\frac{a_0^3}{\bar{n}_{\mathrm{e}}}. \tag{2.31}$$

It is now interesting to compare equation 2.31 to the laser energy deposited upon the plasma surface and therefore consider what fraction of the laser energy can be absorbed via the ZVP mechanism. Using $E = E_{\mathrm{L}}$, equation 2.31 can be rewritten as

$$U_{\mathrm{ZVP}} = \frac{1}{2\omega_{\mathrm{L}}S}\sigma c\epsilon_0 E_{\mathrm{L}}^2. \tag{2.32}$$

For the case of normal incidence, bunches are produced at a frequency of $2\omega_{\mathrm{L}}$, naturally following the frequncy of the $\mathbf{J} \times \mathbf{B}$ force. Assuming a sinusoidal plane wave incident with surface area σ, the energy available during the pushing phase (a quarter cycle) is

$$U_{\mathrm{L},1/4} = \sigma\frac{T}{4}\langle I_{\mathrm{L}}\rangle = \frac{2\pi}{8\omega_{\mathrm{L}}}\sigma c\epsilon_0 E_{\mathrm{L}}^2. \tag{2.33}$$

Hence,

$$\eta_{\mathrm{ZVP}} = \frac{U_{\mathrm{ZVP}}}{U_{\mathrm{L},1/2}} = \frac{2}{\pi S}. \tag{2.34}$$

Interestingly, this new analytical result predicts the trend observed by A. Savin [7] in PIC simulations both in magnitude and in scaling. Indeed, A. Savin demonstrated

$$\eta_{\mathrm{ZVP}} \sim S^{-1.000(3)}, \tag{2.35}$$

however, this result led A. Savin to conclude that increasing S reduces absorption, increasing the energy in the reflected HHG beam thus increasing high harmonic efficiency, seemingly in tension with the vast majority of the work on this process [CITE CITE CITE]. The resolution arises from awareness of two distinct conversion efficiencies that describe the reflected harmonic spectrum: the conversion efficiency into the whole reflected beam and the conversion efficiency for individual harmonics. While the total conversion into the reflected beam decreases for decreasing S, the slope of the harmonic spectrum also decreases, reducing HHG efficiency. Indeed, high X-ray harmonic efficiency neccesitates high reflection inefficiencies due to the production of ZVP electron bunches as higher energy bunches produce more coherent reflected radiation, a caveat not often considered in the quest for higher-order harmonics. The impact of the ZVP mechanism on HHG will be discussed in great detail in the following chapter.

The expressions for energies in equations 2.28 and 2.31 require the electron bunch to fully discharge the pseudo-capacitor before interaction with the subsequent laser pulse peak. Since the electron bunch travels at speed $\approx c$, the peak displacement (and thus the pseudo-capacitor width) must satisfy

$$\Delta x \leq \frac{\lambda}{8}. \tag{2.36}$$

Using equation 2.26, it is clear equation 2.36 is satisfied for $S \geq 1.3$.

2.2.2 ZVP bunches oblique incidence scaling and internal bunch structure

This section is inspired by ideas from the work of Gonoskov *et al* [9] and VIncenti *et al* [12] to extend the theory of the ZVP mechanism for energy absoption to the more practical[1] case of oblique incidence.

****The below section needs cleaning up of minus signs etc, take the convention laser propagates in the positive direction therefore drift of electrons and ions in frame with normal incidence is in negative direction.****

[1]Not only is this more feasible in experiment but has been shown to optimise HHG.**CITE**

Provided the plasma-vacuum boundary is sufficiently steep, the plasma electrons will respond adiabatically to the laser pulse and arrange themselves to form a pseudocapacitor longitudinal electric field E_{C} at the plasma surface. At all points in this adiabatic 'pushing' phase, the surface electrons will be in a quasi-static equilibrium *i.e.* there will be a balance between the electromagnetic forces on them. Consider again the laser pulse incident on a solid density plasma existing for $x > 0$ at angle θ. Transforming to the frame of reference in which the laser is normally incident (quantities in this frame are indicated by the primed symbol), the electron and ion bulk plasma species stream at velocity $\mathbf{v}_{\mathrm{d}} = -c\sin\theta\hat{\mathbf{y}}$. Applying the Lorentz force law along the longitudinal direction ($\hat{\mathbf{x}}$), for a displacement of the electron fluid x'_{e} (one assumes that the expression for a single electron at the surface describes the surface since all electrons follow similar trajectories), travelling at speed $\mathbf{v}'$,

$$-e(\mathbf{v}'(x'_{\mathrm{e}}) \times (\mathbf{B}'_{\mathrm{L}}(x'_{\mathrm{e}}) + \mathbf{B}'_{\mathrm{i}}(x'_{\mathrm{e}})) \cdot \hat{\mathbf{x}} + E'_{\mathrm{C}}(x'_{\mathrm{e}})) = 0, \tag{2.37}$$

where the laser magnetic field,

$$B'_{\mathrm{L}} = \frac{m_{\mathrm{e}}\omega'_{\mathrm{L}}a_0\sin(\omega'_{\mathrm{L}}t' - k'x'_{\mathrm{e}})}{e}\hat{\mathbf{z}} \tag{2.38}$$

and B_{i} is the magnetic field generated by the uncompensated ion current, $\mathbf{J}_{\mathrm{i}} = Zen'_{\mathrm{i}}(x'_{\mathrm{e}})\mathbf{v}_{\mathrm{d}}$, where the electron fluid has been displaced. As before, from equation 1.9,

$$E'_{\mathrm{C}} = \frac{en'_{\mathrm{e}}x'_{\mathrm{e}}}{\epsilon_0}. \tag{2.39}$$

Note that there is no contribution to the laser magnetic field here from the reflected laser pulse since the assumption is that during this pushing phase all laser pulse energy is converted into electrostatic potential energy, this is supported by the attosecond duration of the reflected harmonic beam (*i.e.* it is not produced during this phase). Maxwell-Ampère's Law states

$$\nabla \times \mathbf{B} = \mu_0\mathbf{J}. \tag{2.40}$$

Noting that by symmetry there can be no variation in the magnetic field with y' or z' it becomes clear that

$$-\frac{\mathrm{d}(\mathbf{B}'_{\mathrm{i}})_{z'}}{\mathrm{d}x'} = \mu_0(\mathbf{J}_{\mathrm{i}})_{y'}. \tag{2.41}$$

Integrating equation 2.41 from $-\infty$ to x'_e, noting that $\mathbf{B}_\mathrm{i} = 0$ at infinity and assuming a constant density profile n'_i for $x > 0$,

$$\mathbf{B}'_\mathrm{i}(x'_\mathrm{e}) = \mu_0 e n'_\mathrm{e} x'_\mathrm{e} c \sin(\theta)\hat{\mathbf{z}}. \tag{2.42}$$

Using equations 2.38, 2.39 and 2.42 and making the very reasonable approximation that the relativistic electrons on the surface move at speed $v'_y \approx \pm c$ at peak displacement ($x'_\mathrm{e} = x'_\mathrm{p}$), 2.37 can be written as

$$-e\left(\pm c\left(\pm\frac{m_\mathrm{e}\omega'_\mathrm{L}a_0}{e} + \mu_0 e n'_\mathrm{e} x'_\mathrm{p} c \sin\theta\right) + \frac{e n'_\mathrm{e} x'_\mathrm{p}}{\epsilon_0}\right) = 0. \tag{2.43}$$

Note that to be in the laser pushing phase the first term must be negative, corresponding to $\mathbf{v}'$ and $\mathbf{B}'_\mathrm{L}$ having the opposite sign, hence,

$$c\left(-\frac{m_\mathrm{e}\omega'_\mathrm{L}a_0}{e} \pm \mu_0 e n'_\mathrm{e} x'_\mathrm{p} c \sin\theta\right) + \frac{e n'_\mathrm{e} x'_\mathrm{p}}{\epsilon_0} = 0, \tag{2.44}$$

where here the $\pm$ tracks the sign of $\mathbf{v}'$. After some maniputation, one arrives at

$$x'_\mathrm{p} = \frac{1}{k'S'(1 \pm \sin\theta)}. \tag{2.45}$$

Transforming back to the lab frame, naturally,

$$x_\mathrm{p} = \frac{1}{kS(1 \pm \sin\theta)}. \tag{2.46}$$

Already this is quite a result, reducing to equation 2.26 for $\theta = 0$ and predicting the suppression and enhancement of the two surface oscillations per laser puse cycle. Explicitely, for a laser pulse propagating at $y = x\tan\theta$, the peak displacement of the electron surface is enhanced for $\mathbf{B}_\mathrm{L}$ in the $+\hat{\mathbf{z}}$-direction and suppressed for $\mathbf{B}_\mathrm{L}$ in the $-\hat{\mathbf{z}}$-direction.

Consider now acceleration of the electron bunch across the pseudocapacitor field in the boosted frame,

$$T' = \int \mathbf{F}' \cdot \mathrm{d}\mathbf{s}' = \int_{x'_\mathrm{p}}^{0} -eE'_\mathrm{C}(x'_\mathrm{e})\mathrm{d}x'_\mathrm{e} = \frac{e n'_\mathrm{e}(x'_\mathrm{p})^2}{2\epsilon_0} = \frac{1}{2}m_\mathrm{e}c^2\frac{a_0^2}{\bar{n}'_\mathrm{e}(1 \pm \sin\theta)^2}. \tag{2.47}$$

Again, transforming back to the lab frame, noting the gain in energy from crossing the pseudo-capacitor

The linearity of four-vectors ensures

$$\mathbf{\Delta P}^{\mu} = (\frac{\Delta E}{c}, \mathbf{\Delta p}) \tag{2.48}$$

is also a four-vector. The Lorentz transform for change in energy is thus

$$\Delta E = \gamma \left(\Delta E' - \frac{\mathbf{v}_{\mathrm{d}}}{c} \cdot \mathbf{\Delta p}' \right), \tag{2.49}$$

where

$$\gamma = \frac{1}{\sqrt{1+\sin^2\theta}} = \frac{1}{\cos\theta}. \tag{2.50}$$

Hence for energy gain $\Delta E' = T'$ in the boosted frame (where $\Delta p_y = 0$),

$$T = \gamma T'. \tag{2.51}$$

Using equations 2.47 and 2.50 and recalling $\bar{n}_{\mathrm{e}} = \bar{n}'_{\mathrm{e}}/\gamma$,

$$T = m_{\mathrm{e}} c^2 \frac{a_0}{2S(1 \pm \sin\theta)^2} \tag{2.52}$$

Nb this could have simply been established in the lab frame and considering F.ds which is just the same[The electron bunch then accelerates across the pseudo-capacitor in the specular direction, the force] maybe put this derivation in appendix.

Also note that when doing this transformation, T is the energy gained but there is another term in the momentum from the transform, since now $v_y = c \sin\theta$. This is unrelated to the energy gain from crossing the pseudo capacitor. There is no explanation of where this energy comes from, just that in order for the bunch to travel in the -x direction in the boosted frame - not sure what real explanation there is for this to occur, also confusion here since is this actually contained within the gamma expression or not, im lost come back to this. Maybe actualyl this is fine. We jsut take the gamma factor associated with the py gain ($= \sec\theta$ - corresponding to a gamma of 1.4 at 45 degrees) and add the delta gamma from the pseudo capacitor and that should be fine.

Another note: this dependence on theta $(1 \pm \sin\theta)$ can be explained as an increase due to the electric field having a component acting either in or out from the plasma surface either assisting or counteracting the magnetic field.

Idea: Can one use an external constant magnetic field to obtain the same results for normal incidence?

Also need to go back through this section and make clear which gamma is which in this section

Therefore, as with peak displacement, the energy gained by the electron bunch via the ZVP mechanism is suppressed in one half cycle and enhanced in the second.

While this model would suggest an optimal angle for electron energy and therefore HHG of $\pi/2$, if $\theta > \pi/4$, then, if the relativistic electron bunch is travelling at c along the specular reflection direction, the subsequent laser peak amplitude will never 'catch up' with the electron bunch, and electrons will escape through the antinodes (?) of the electric field [CITE KRUSHELNICK PAPER GRAZING INCIDENCE ELECTRONS], generating high charge electron bunches in reflection, but decreasing **HHG efficiency!** (**HHG efficiency!**).

Finally, moving on to the calculation of total bunch energy as a function of θ. Since the total number of electrons in the accelerating bunch must be invariant,

$$U_{\mathrm{ZVP}}(\theta) = n_{\mathrm{e}}\sigma\Delta x T(\theta) = \frac{\sigma n_{\mathrm{e}}}{k} \times m_{\mathrm{e}}c^2 \frac{a_0}{2S^2(1 \pm \sin\theta)^3}. \tag{2.53}$$

What we can see from this is this enables a larger fraction of the laser energy to be absorbed at high S pushing the currently experimentally accessible regime into the most efficient regime.

I want to move on, but return to this section and sort out the following.

Another concern: peter showed me sims that suggested that increasing S incerased the suppressed oscillations more RELATIVE to the main oscilisations, perhaps need to look at the internal bunch structure?

Also see if can do a second order calculation through the electron bunch to see if can calculate its structure.

Big note: The highest electron gamma factors comes from those electrons at the very front surface who are accelerated before high density is reached and quasistatic equilibrium reached (there are therefore very few of them), these few electrons do not satisfy ZVP relation for energy, instead ponderomotvie + ZVP which at most would be twice the predicted gamma which is quite some difference HOWEVER for all experiments so far, ZVP energy gain is small since S large so ponderomotive is more sensible.

Earlier write something along the lines of explaining while ZVP absorption does represent laser energy absorption, bulk heating occurs rather indirectly.

2.3 Defining characteristics of the ZVP mechanism

In the original paper on the ZVP mechanism, T. Baeva *et al* [5] outlined 6 defining characteristics of the ZVP mechanism, namely,

1. The existance of vector potential zeros moving through the skin layer in the laboratory frame;
2. The existance of zeroes in the incident laser pulse vector potential required for the formation of fast electron bunches;
3. The generation of fast electron bunches with ultra-short temporal duration;
4. That such fast electron bunches follow the energy scalingings of equations **??** and total energy **??**;
5. Injection of the fast electron bunches is along the propagation axis of the laser pulse;
6. There must be an intrinsic link must exist between the fast electron bunches and coherent X-ray HHG;

with the moving zeros within the skin layer being the defining delineator between this post-ponderomotive regime of laser pulse energy absorption and all other proposed mechanisms. While such observational requirements are far beyond the reaches of currently experimental know-how, numerical simulations in both 1- [5] and 2-dimensions [6] have confirmed the above points. Now is presented the first 3D simulations attempting to demonstrate these criteria.

2.4 Numerical simulations of the ZVP mechanism

This thesis relies on the analysis of 1,2 and 3D PIC simulations, primarily using the massively-parallel and open-source simulation code Smilei [3]. Simulation parameters will be provided throughout. ****Discuss choice of S parameter somewhere. Also note that these parameters are currently accessible on ELI-NP.****

2.4.1 The ZVP mechanism in 3D3V

The 3D simulation results are presented in figure 2.3 alongside comparison to an equivalent 2D simulation. Simulation parameters in table 2.1, such parameters are compatible with the 10 PW ELI-NP state-of-the-art laser facility [13]. Figure 2.3c) clearly demonstrates the existence of high energy density electron bunches propagating through the plasma bulk in the direction of the laser pulse. Note that this ZVP criterion is required by conservation of transverse momentum inside the plasma bulk where the laser fields cannot propagate. Figure 2.3b) shows these bunches escape to the rear of the bulk but lose energy as they do so. Looking now at figure 2.3e) and the internal structure of the plasma bulk. These bunches drive two-stream and filamentation instabilities [14]. The bulk propagating bunches are accompanied by higher density electron buches to either side of the plasma block with the side switching every half laser pulse cycle.

The plasma specifications were chosen to minimise computational load while ensuring numerical convergence, requiring over 100 billion macroparticles. The electron temperature is raised significantly higher than that which would be expected in such a laser-plasma system so as to resolve the Debye length. Anticipated plasma temperatures are calculated using 1D HYADES simulations in the following chapter. While this temperature is unphysical and will lead to some small plasma expansion over course of the simulation, the temperature remains negligible compared to that imparted to the electron bunches by the laser pulse. The striking similarity between the 2 and 3D simulation results is a natural consequence of the 2D nature of the interaction geometry. It is however still reassuring to note that previous work withstands the stringent test of the real universe geometry.

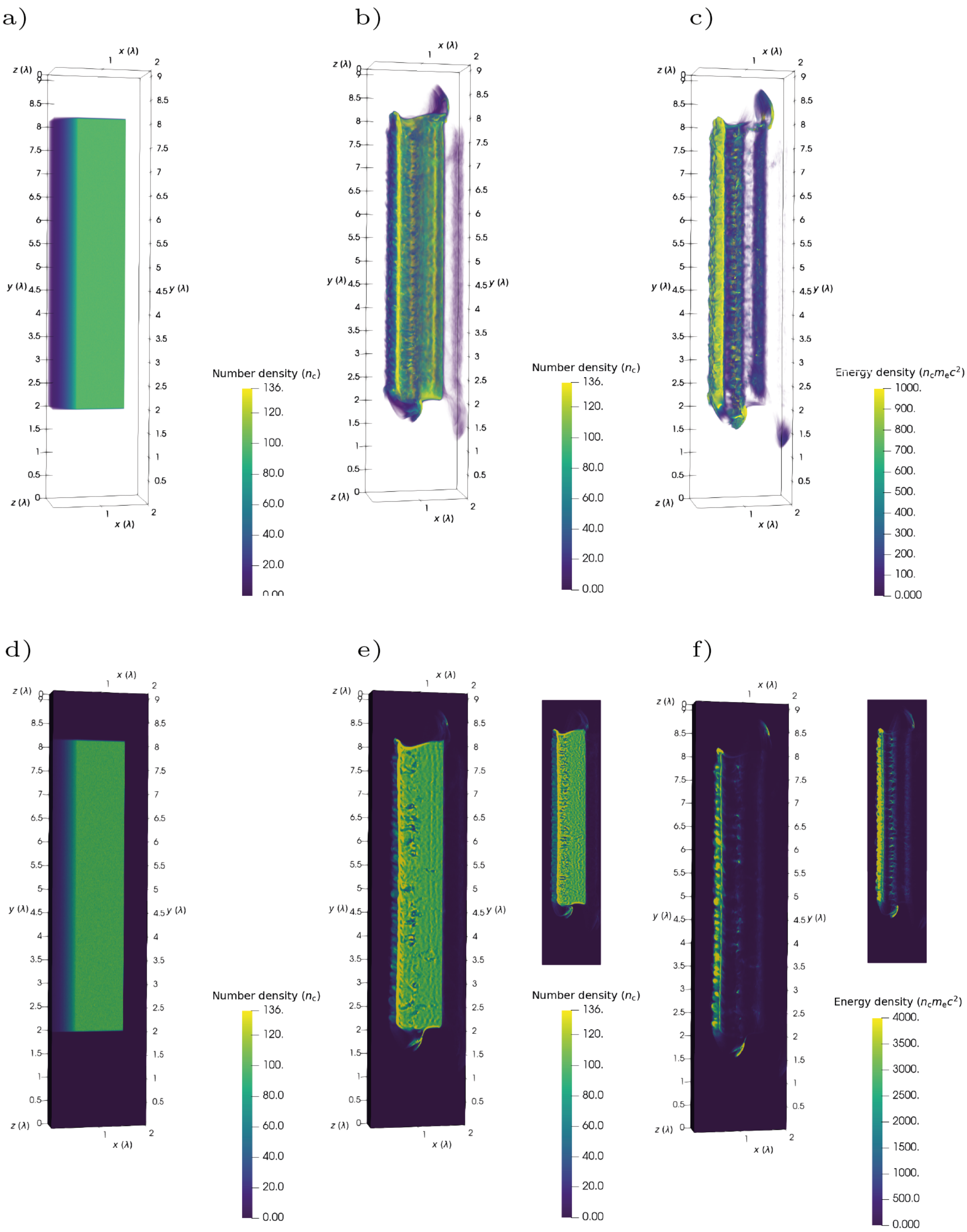

Figure 2.3: Simulation results from a 3D PIC simulation of the ZVP mechanism. a) The initialised electron number density. b) The electron number density several cycles later, the plasma bulk is intact, however there is evidence of instabilities and electron bunches propagating through and around the plasma. c) The electron kinetic energy density at the same timestep. Note that the scale has been clipped to enable observation of both electron bunches propagating through and around the plasma bulk. Significantly higher energy density, corresponding to a higher charge density and attosecond duration for the electron bunches propagating around the bulk. d-f) Plots clipped through $z = 0$ for a-c) respectively for better clarity on the internal structure of the plasma bulk. The accompanying plots for figures e) and f) are corresponding 2D PIC simulation results.

Laser (3D, normal incidence)		
Parameters	Real	Sim
Wavelength, λ (nm)	1060	2π
Angular frequency, ω_L (fs^{-1})	1.8	1
Beam waist, L_0 (nm)	6λ	12π
Focal point, $(f_x,\ f_y,\ f_z)$ (nm)	$(0.5\lambda,\ 5\lambda,\ 0.5\lambda)$	$(\pi,\ 10\pi,\ \pi)$
Spatial envelope, E_i, $i = y, z$	$E_i \sim e^{-(i-f_i)^2/L_0^2}$	
Temporal envelope, E_t	$E_t \sim e^{-(t-4\lambda/c)^2/(4\lambda/3c)^2}$	
Simulation box		
Size, $x \times y \times z$ (nm)	$2\lambda \times 9\lambda \times \lambda$	$4\pi \times 18\pi \times 2\pi$
Sim length (fs)	35.22	20π
Spatial resolution, Δx (nm)	$\lambda/128 = 8.28$	0.0491
Temporal resolution, Δt (as)	$\Delta x/11c = 2.51$	0.00446
Collisionless, pre-ionised randomly-initialised aluminium plasma		
Electron x profile, $n(x)$	$\begin{cases} n_e \text{ for } 2\lambda \le x \le 3\lambda, \\ n_e e^{(x-2\lambda)/0.2\lambda} \\ \quad \text{for } x \le 2\lambda. \end{cases}$	
Electron y profile, $n(y)$	$\begin{cases} 1 \text{ for } 2\lambda \le y \le 8\lambda, \\ 0 \text{ otherwise.} \end{cases}$	
Electron z profile, $n(z)$	$\begin{cases} 1 \text{ for } 0.125\lambda \le y \le 0.875\lambda, \\ 0 \text{ otherwise.} \end{cases}$	
Ion profile, $n_i(x, y, z)$	$n_i = n(x)n(y)n(z)/13$	
Macro-electrons per cell	729	
Macro-ions per cell	8	
Ion temperature, T_i (keV)	0	0
Electron temperature, T_e (keV)	10	0.02
Stability criteria		
$\lambda_D/\Delta x$	0.288	
$1/\Delta t\omega_p$	24.4	
Macro-particles in the Debye sphere	210	

Table 2.1: Simulation parameters in both real and normalised Smilei simulation units for the 3D3V simulations.

Convergence of 3D simulations

The 3D simulation parameters were chosen to be consistent with previous work on the ZVP mechanism, however, such simulations are cumbersome, limiting the number of simulations it is feasible to run. In order to query the defining characteristics outlined by Baeva, a lower resolution simulation was performed with similar parameters to the initial simulation. The two simulations are compared in figure 2.4. Good convergence is qualitatively demonstrated by the presence of characteristic features of the ZVP mechanism. While the instabilities are similar in structure, the change in seeding changes their exact positions. As instabilities are not the focus of this thesis this variation is of no concern.

Following the success in reproducing the key features of the ZVP mechanism and demonstrated consistency between 2 and 3D equivalent simulations, the remainder of this chapter will predominantly utilise 2D simulations to interrogate the mechanism further.

2.4.2 The ZVP electron bunch

Previous work on the ZVP mechanism has highlighted the high energ and short duration of electron bunches, however, until now much of the quantitative discussion of the properties of such bunches has avoided interrogation. A ZVP electron bunch is an electron bunch produced via the ZVP mechanism. Once produced and accelerated across the pseudocapacitor field, it is launched back in the laser propagation direction. While the bunch has no spatial separation over energies when propagating with the zero of the vector potential, the turning point of the electrons is longitudinal momentum dependent due to the Coulomb attraction of the ions after overshooting the pseudocapacitor field. Baeva *et al* showed that the electron bunch has a quasi-monoenergetic spectrum: there is a one-to-one relationship between energy and position with the higher energies trailing the lower energies. The full bunch is confined to 130 as while a single energy confined to 5 as. If, however, the plasma bulk is transversely mass-limited relative to the laser spot size,when rotated back towards the plasma block, some of the electron bunch will overshoot and escape the

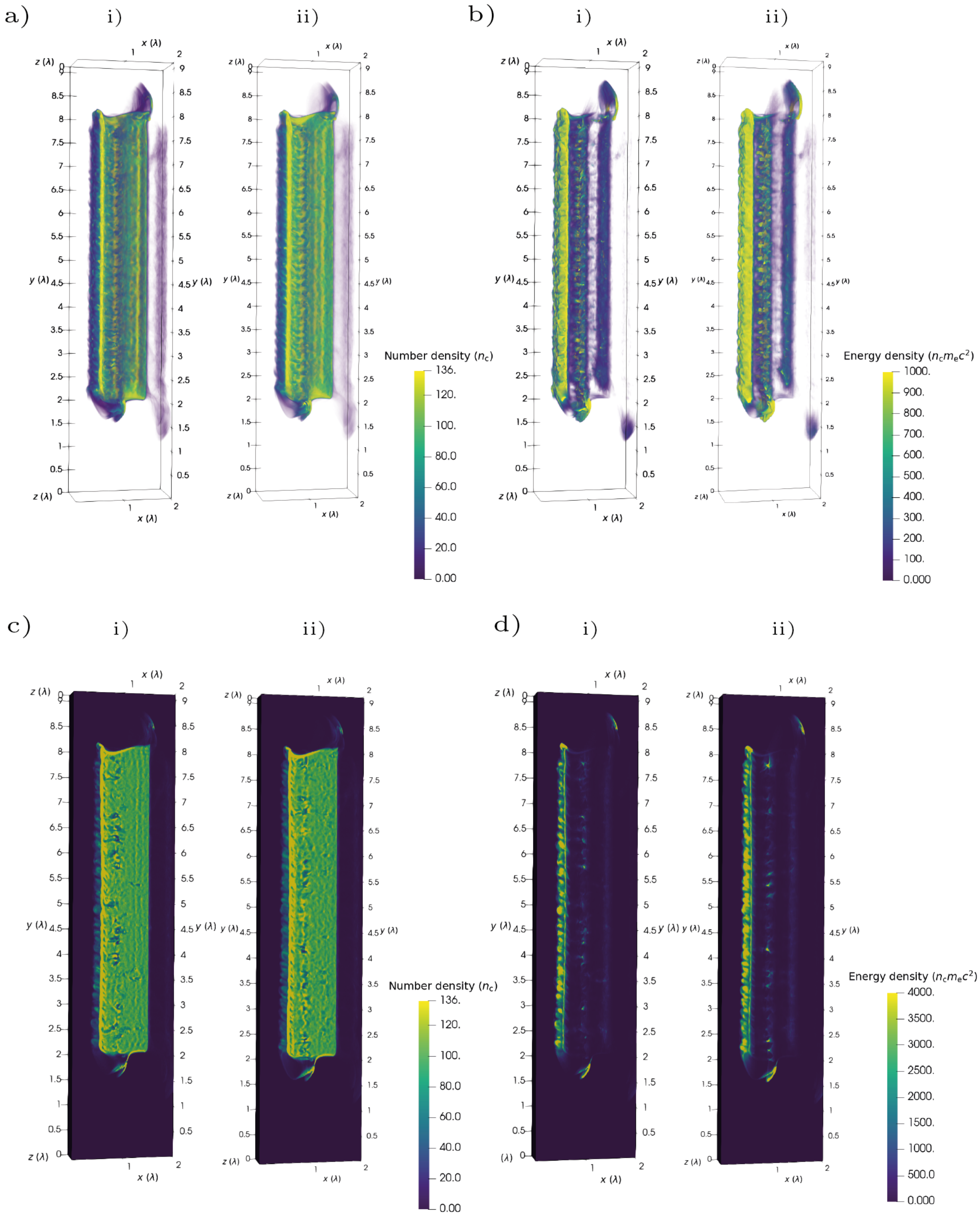

Figure 2.4: Comparison between the initial 3D simulation and a lower resolution version. a) Electron number density. b) Kinetic energy density. c) and d) are slices of a) and b) respectively. *i)* Initial simulation. *ii)* Lower resolution simulation. Good convergence is demonstrated.

potential well without significant stretching of the bunch in time as can be seen in figure 2.3. Such electron bunches (retain the initial energy spread???? ie fast first as disucssed in RES paper) retain their high charge density and ultra-short duration. ZVP electron bunches can therefore be placed into two categories: ultra-high charge, ultra-short duraction electron bunches from mass-limited targets, hereafter labelled mass-limited electron bunches, of interest due to their unique properties and bulk propagating bunches, hereafter labelled bulk bunches, which have lower charge densities, are imprinted with instabilities and are instead of interest due to their connection to energy absorption and reflection in this post-ponderomotive regime.

To investigate these two bunch types further, 2D PIC simulations were performed, see appendix for parameters. Figure blah is reprentative.

Attosecond nano-Coulomb mass-limited electron bunches

Figure 2.5 describes a typical mass-limited ZVP electron bunch qualitatively. The electron bunch under interrogation is ultra-relativistic with a mean energy of 51(11) MeV and a duration of 35 as. It propagates at an angle of -393 rad relative to the laser propagation direction, *i.e.* the x-axis, and a transverse geometric emittance in the simulation plane (the x-y plane) of 35(7) nm rad. A definition of the transverse geometric emitance, a measure of the quality of the electron beam, is given in appendix A.2. Note that while the bunch does not propagate in the laser propagation direction, this does not mean it must be rejected under consideration of the ZVP bunch conditions. Indeed, the bunch must propagate at some angle to the laser since conservation of canonical momentum while it remains in thrall of the laser pulse it must have some transverse component of momentum. The more standard ZVP bunches passing through the bulk again by conservation of momentum must propagate along the axis, as is observed in simulation. For an equivalent bunch in a corresponding 3D simulation, the transverse geometric emittance in the z plane is 15(11) nm rad. This electron bunch has a total charge of 0.35 nC for a slab of plasma of thickness 0.75λ in the z-direction. Noting again

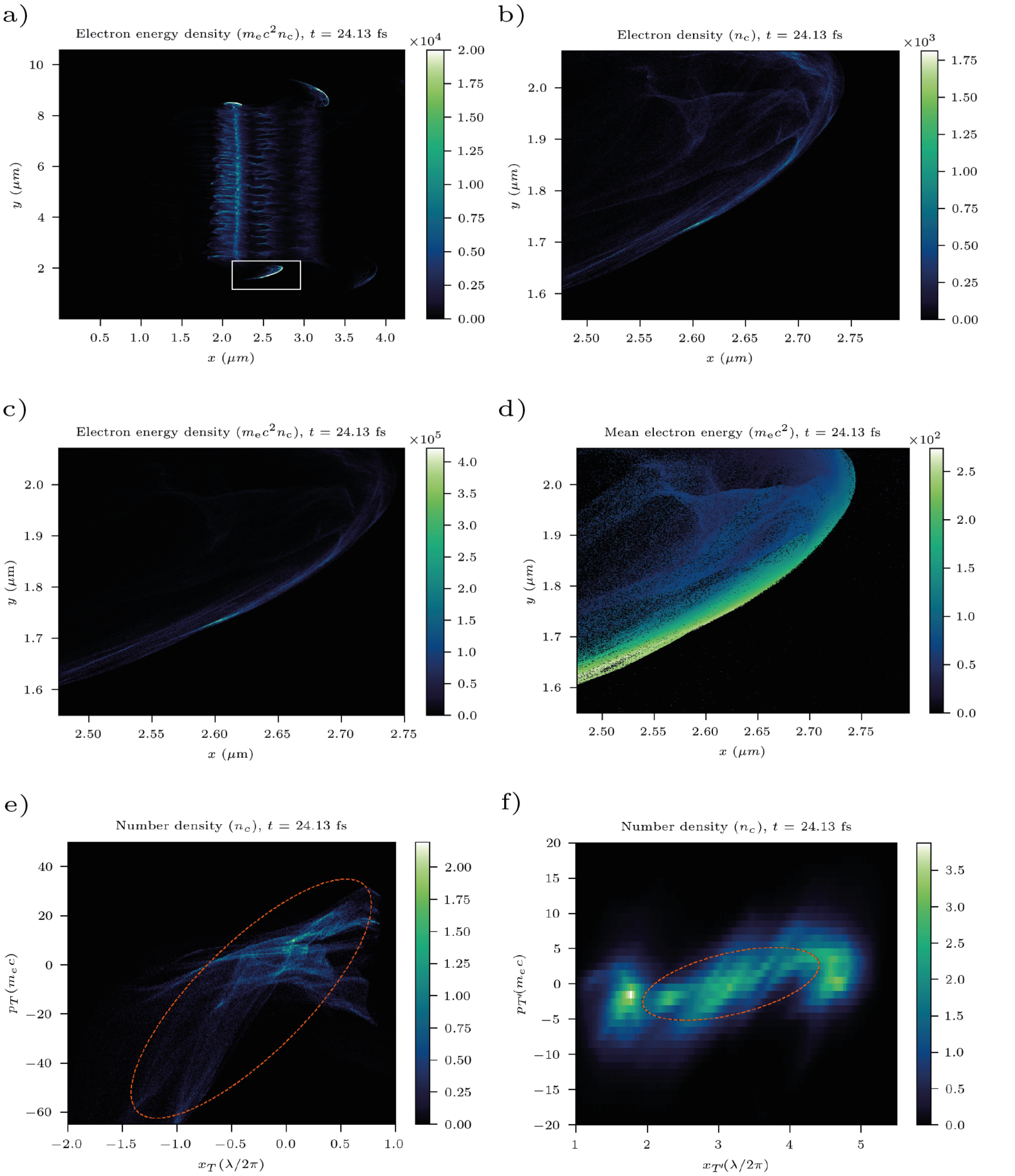

Figure 2.5: 2D PIC simulation results qualitatively describing typical mass-limited ZVP electron bunch structure. a) Electron energy density for the full simulation window, corresponds to figure 2.3f). The box highlights the bunch presented in the following plots. b) Electron number density of the electron bunch. c) Electron energy density of the electron bunch, the colourbar scale has been increased compared to figure a) to demonstrate the internal structure. d) The mean electron energy across the electron bunch, suggesting a position dependent energy or quasi-monoenergetic nature to the electron bunch [5]. Cells with no macroparticles are black. e) The transverse phase space in the 2D simulation plane. The ellipse describes the calculated emittance. The skew of the ellipse is a consequence of a low density tail on the phase space beyond the bottom left corner. f) This plot was extracted from the equivalent 3D simulation and describes the transverse emittance in the z-direction. Again the ellipse marks the emittance. The relatively well-defined border to the phase space and the mild tilt (indicating only mild divergence) are direct consequences of the 2D nature of the interaction.

the two-dimensional nature of the interaction geometry, and that electrons less than twice the relativistic Larmor radius,

$$r_\mathrm{l} = \frac{\gamma m_\mathrm{e} v}{eB}, \tag{2.54}$$

where γ and v correspond to the electron velocity and B is the magnetic field of the laser pulse, when rotated back towards the plasma will escape to the side, the total number of electrons in the mass-limited bunch is

$$N = 2 n_\mathrm{e} r_\mathrm{l} L_z \Delta x, \tag{2.55}$$

where L_z is the width of the plasma in the z-direction. Using equation 2.26 for Δx and 2.50 for γ and approximating $v \approx c$ for the ultra-relativistic electron bunch,

$$N = 2\gamma n_\mathrm{c} \frac{L_z}{k^2}. \tag{2.56}$$

For these simulation parameters, this corresponds to a total bunch charge, $Q = eN$, of 0.37 nC, a remarkably successful prediction of the ZVP model. Equation 2.56 tells us there is no limit to the

Equation 2.56 can be rewritten in terms of fundamental constants as

$$N = 2(1 + 0.5\frac{a_0^2}{\bar{n}_\mathrm{e}}) L_z \frac{m_\mathrm{e} \epsilon_0 c^2}{e^2}. \tag{2.57}$$

Almost counterintuitively, it would appear the total charge scales inversely with the plasma density. Instead, charge can be increased either by increasing the laser pulse intensity or L_z. Indeed, provided the laser pulse intensity remains relativistic, the focal spot can be increased indefinitely and there is no limit to the mass-limited electron bunch total charge. For a realistic laser pulse with beam width 10λ incident on a larger laser block, equation 2.57 predicts a charge of 9.3 nC.

Discuss use cases of the electron bunches. DIscuss if bunch quasi-monoenergetic.

Figure blah blah compares the electorn bunch energy to an equivalent[2] bunch produced by a circularly polarised laser pulse. The mean electron bunch energy is over three times lower as there is no ZVP acceleration phase and there is no quasi-monochromatic nature [5].

[2]A circularly polarised laser pulse will expel electrons from a mass-limited target in a corkscrew shape, the bunch is therefore only loosely equivalent.

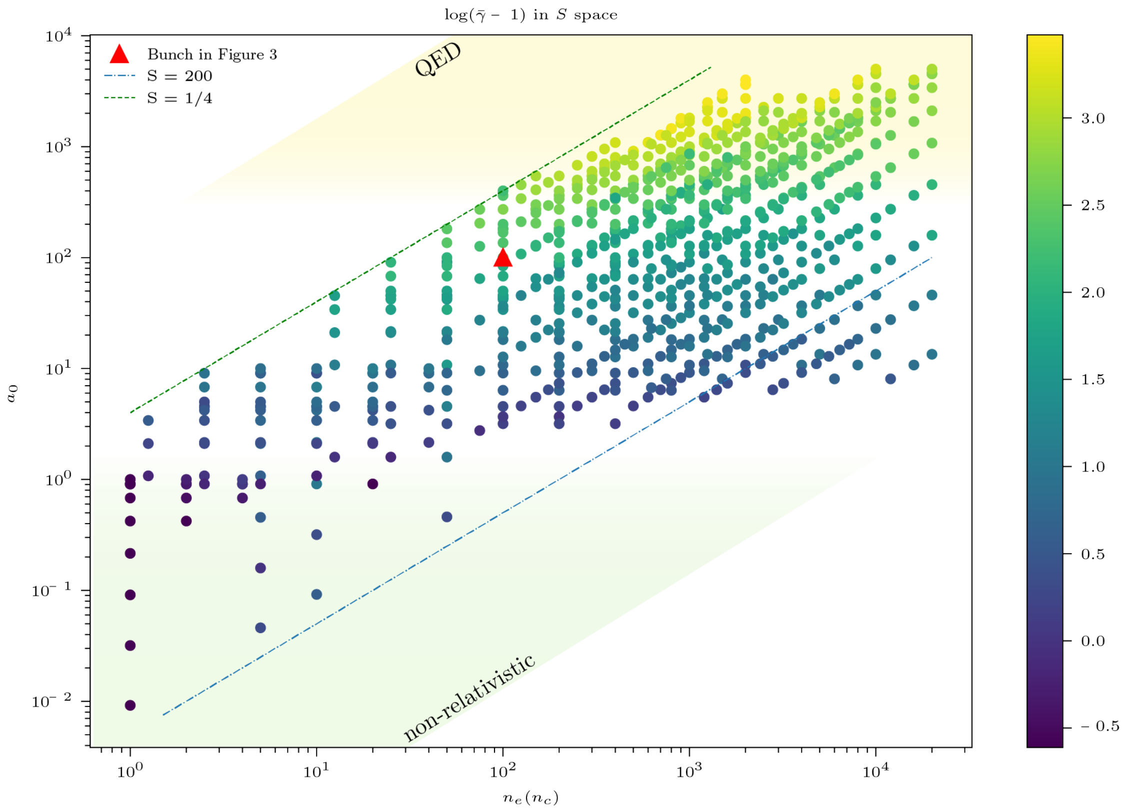

Figure 2.6: Mean mass-limited ZVP electron bunch normalised kinetic energies extracted from 2D PIC simulations. The bunch detailed in figure 2.5 is highlighted.

Parameter scan of electron bunch mean energy

Since ZVP energy scaling is a fundamental identifier of ZVP bunches, it is important to confirm that mass-limited electron bunches follow the same scaling relations as has previously been confirmed for bulk ZVP electrons in both 1D [5] and 2D [6] PIC simulations. The mean mass-limited electron bunch kinetic energies were extracted from 120 2D PIC simulations and are plotted in figure 2.6. The dependence on both a_0 and n_e demonstrates these electron bunches are accelerated by a non-pondermotive mechanism. The parameter scan ranged plasma block density ranging from the critical plasma density to well-beyond solid density for the aluminium target and with laser pulse peak intensity ranging from non-relativistic ($a_0 < 1$) through to the Quantum Electro-Dynamics (QED) plasma regime ($a_0 > 300$) up to a peak $a_0 = 5000$ to investigate the change in scaling observed by Savin *et al* [15] at the onset of QED effects. This study is also the first to extract specific bunch energies as opposed to total simulation box energy gain, representing a far more stringent test of ZVP theory.

Care must be taken however as the energy of such electron bunches cannot be directly compared to the ZVP energy relations as as aforementioned after escaping the potential, the electron bunch experiences further direct laser acceleration before reaching the detection point. Indeed, Thévenet *et al* [16] suggested that attosecond electron bunches produced in reflection exhibit precisely the phase and energy properties required to 'surf' the reflected laser pulse and experience vast acceleration gradients over the Rayleigh length of the laser pulse. This process is known as Vacuum Laser Acceleration. It seems highly likely that this process occurs for electron bunches produced in transmission. This seemingly unfortunately situation in reality provided a fully optical scheme to create GeV nano-Coulomb electron bunches from the most simple of setups: a laser interacting with a mass limited solid target (thus reducing the alignment complexity.).

Returning to the determination of the electron bunch energy at the measurement point, consider now the journey of the electron bunch after expulsion from the plasma bulk. It is rotated back towards the plasma bulk by the magnetic field of the subsequent peak of the laser pulse, then travelling at approximately c it surfs the peak, experiencing an approximately constant accelerating electric field from the laser pulse at some fraction f of the laser field peak. The work done by this field is then

$$\Delta T = \int e\mathbf{E} \cdot \mathrm{d}\mathbf{x}. \tag{2.58}$$

Note that for this process, the laser pulse electric field and electron bunch direction of travel will always be aligned no matter to which side of the plasma bulk the electrons are accelerated to and therefore ΔT will always increase the energy of the electron bunch, thus,

$$\Delta T = efE_{\mathrm{L}}\Delta y, \tag{2.59}$$

where Δy is the distance along y from the plasma edge to the detection point. Accounting for the Gaussian spatial profile of the laser, $a(t) = a_0 \exp(-y^2/(6\lambda)^2)$ at focus, the gamma factor after both acceleration phases for this simulation setup is then

$$\gamma = 1 + (0.30) \times \frac{a_0^2}{\bar{n}_\mathrm{e}} + (1.2f) \times a_0'. \tag{2.60}$$

Here the primed vector potential refers to the intensity of the subsequent peak of the laser pulse. This final term could be neglected or at least reduced somewhat once super-Gaussian spatial laser pulses become standard in this intensity regime or using a suitable plasma separator [**miyauchi_2004_LaserElectronAcceleration**]. Both acceleration phases fail to meet the criteria of the Lawson-Woodward theorem. The ZVP phase is dependent on the existence of electrostatic forces, while the secondary phase occurs for a finite interaction region.

Fitting equation 2.60 to the PIC simulation data presented in figure 2.6 finds

$$\gamma = 1 + (0.46 \pm 0.02) \times \frac{a_0^2}{\bar{n}_\mathrm{e}} + (0.28 \pm 0.01) \times a_0' \tag{2.61}$$

with an r^2-value of 0.818. This fit suggests $f = 0.22 \pm 0.01$. The electric field experienced for a random selection of electrons in a bunch was extracted from one simulation. Encouragingly, the mean attenuation of the electric field they experience is 0.20 ± 0.05, to calculate this attenuation directly falls beyond the scope of ZVP theory.

This is the first demonstration of ZVP theory to calculate actual values and not only the scaling relationship. Such order of magnitude calculation is essential to compare this model of absorption to others and thus determine the dominant mode for absorption. It is certainly remarkable that such a simple theory for energy absorption has such predictive success in this highly non-linear and seemingly chaotic many particle system. It is interesting that increasing laser intensity to such extremes will, at least for a short time, cause relativistic effects that add coherency to electron motion before total annihilation of a target.

The relative error between data and theory is plotted in figure 2.7. Those points marked by an orange triangle have associated errors of over an order of magnitude.

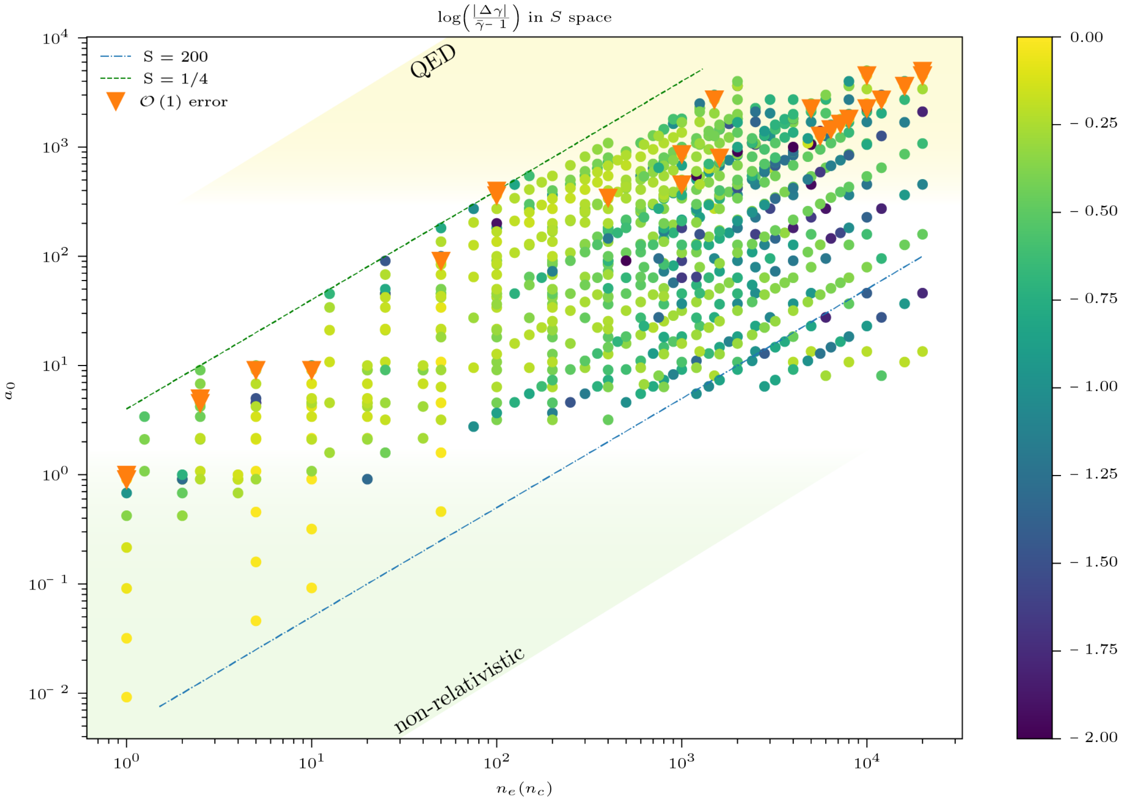

Figure 2.7: The relative errors for each mean energy data point compared to figure 2.6. The orange triangles indicate data points for which the model fails to predict the mean energy.

Reassuringly, such points occur only after the onset of QED effects, known to impact the ZVP mechanism [**savin_2019_EnergyAbsorptionLaserQED**] and for $S < 1$, that is, where the plasma becomes relativistically transparent to the laser pulse, a fundamentally different regime. Equally, for non-relativistic laser intensities, where assumptions of electron coherency cannot be made, are poorly fit by the model. It is particularly interesting that there is no indication that large S causes a breakdown of the model, extending the applicability of the model further than previously considered, opening up the field to a wider range of conditions, such as that of shock compressed plasmas. To summarise, it would appear the ZVP model is valid for $10 \leq a_0 \leq 300$ and $S \geq 1$.

To do: Look again at trajectories Look again at just fitting the region where expression is valid. Temporal effects (non-existant, discuss)

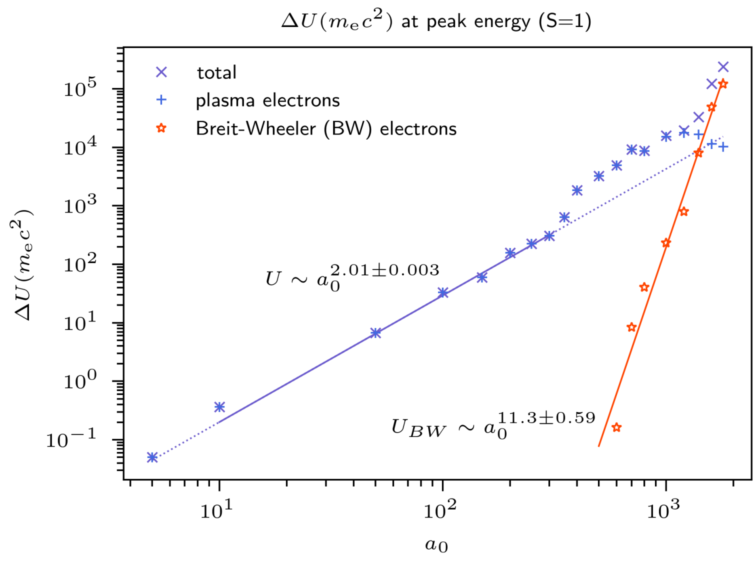

Figure 2.8: Peak instantaneous bulk electron bunch total energy escaping to the plasma bulk rear.

2.4.3 Energy absorption in the ZVP regime

As stated previously the laser-plasma coupling exists in a state of adiabaticity with the exception of the ZVP acceleration phase and hence equation 2.31 describes the absorption of laser pulse energy. For normal incidence, the rate of energy transfer is therefore

$$R = \frac{U\omega_{\mathrm{L}}}{\pi}, \tag{2.62}$$

since two bunches are produced per laser cycle. To demonstrate the scaling for U in 2D PIC simulations, peak instantaneous electron bunch energies escaping to the rear of the bulk were extracted from those PIC simulations with $S = 1$. For constant S,

$$U \sim a_0^2. \tag{2.63}$$

Eneriges are plotted in figure 2.8. Fitting the total energy within the range of validity established for the ZVP model finds

$$U \sim a_0^{2.01\pm0.003}, \tag{2.64}$$

reproducing with great success the anticipated scaling within the ZVP regime. It is also quite satisfying that the number of electrons and bunch mean energies both follow their anticipated ZVP scalings, further evidence this is not a simple ponderomotive effect. By extracting specific bunch total energies, rather than just the peak energies of the plasma block as a whole as was performed in previous studies, this is a far more direct confirmation of energy absorption by the ZVP mechanism into electron bunches. This is highlighted by the difference in results obtained for this study compared to a previous study by Savin *et al* [**savin_2019_EnergyAbsorptionLaserQED**] when investigating the QED regime as will be discussed later. It was not possible to reproduce the constants of equation 2.31 as the neutralising return current in the plasma bulk generates an electrostatic field on the rear side of the plasma block, decelerating bulk electron bunches as they escape the plasma. It should be possible to calculate the deceleration by considering the number of electrons expelled by the plasma. It is however, clear from the simulations that at least some electrons in the escaping bunch are trapped by this rear-side potential well reducing its magnitude.

While equation 2.31 describes energy absorption into hot electron bunches, the coupling of such hot collisionless electrons to the bulk plasma given the lack of collisionality is necessarily indirect. There are two key mechanisms [**sherlock_2014_IndepthPlasma** Firstly, via a cooler resistive return current of electrons that neutralises the current of the injected hot electrons that escape the potential well of the front surface (cite this, the refernce in sherlock 2014 is not great). Since all hot electrons travel at approximately speed c, the magnitude of the return current depends not on the total energy absorbed but instead on the total number of electrons injected, as given by equation 2.30, depending linearly on laser spot area and the electric field magnitude and not on the plasma density[3]. Secondly, via the formation of large amplitude bulk plasma waves induced in the wake of the hot electron bunches. Sherlock *et al* [**sherlock_2014_IndepthPlasmawaveHeating**] calculate the magnitude

[3] Note that for a sufficiently thin target, the return current induces an electrostatic field on the back surface of the target which can then reflect hot electron bunches and decelerate them to the point of a return to collisionality. This is a reality for the PIC simulations explored in this thesis, however, since realistic targets are much thicker this shall be neglected.

of the induced wakefield to be

$$E_{\mathrm{W}} = \frac{eN_{\mathrm{e}}c}{\omega_{\mathrm{p}}\epsilon_0} = \sigma\sqrt{\frac{m_{\mathrm{e}}\epsilon_0}{n_{\mathrm{e}}}}E_{\mathrm{L}}, \tag{2.65}$$

where here the bunch velocity has been set to c, bulk electrons will be accelerated by E_{W} and their kinetic energy converted to heat via collisions. Interestingly, this reproduces the mid temperature electon scaling with density that was observed by Chrisman *et al* [**chrisman_2008_IntensityScalingHot**] in their study of hot electron energy coupling in cone-guided fast ignition of inertial fusion targets. This is a significantly different possible explanation to their self-declared 'hand waving argument'. Excluding this study, such formulations for heat transfer to the plasma bulk within the ZVP regime remain untested in simulations.

Note also that as the laser pulse intensity rises, the fraction of energy absorbed by the ion species increases. Savin [**savin_2019_ModellingLaserPlasmaInteractions**] determined for $S = 1/2$, $a_0 = 100$, that this would be almost 20%. Energy is absorbed by ions via the hole boring mechanism as described elsewhere in this thesis.

2.4.4 Unpacking the QED effects of figure 2.8

In Savin's influential paper [**savin_2019_EnergyAbsorptionLaserQED**], he determined theoretically and demonstrated in simulation that at $a_0 = 300$, $n_{\mathrm{e}} = 50n_{\mathrm{c}}$, there is a transition from standard ZVP scalings to an enhance QED scaling associated with **BW!** (**BW!**) electrons increasing the pseudocapacitor plate charge. Explicitely,

$$T \sim \frac{a_0^5}{\bar{n}_{\mathrm{e}}}. \tag{2.66}$$

Such a scaling shift was not observed for the large parameter scan presented in figure 2.6. Simulations revealed this was likely due to few **BW!** pairs produced towards the plasma edges and hence no additional gain in energy from crossing the pseudocapacitor. Another concern is Savin's study was conducted within the regime of relativistic transparency where it is unclear whether the ZVP potential well can be maintained and was not explored in this study. The final consideration is the well known effect of radiation trapping due to the radiation reaction [17], also observed in these PIC simulations. After acceleration across the pseudocapacitor, the electron bunch encounters the subsequent laser peak. If the electron bunch gamma factor and laser intensity are both large enough (include chi requirement), electrons radiate a significant fraction of their energy and are thus stopped in their tracks. Unable to now escape the potential well at the plasma surface they remain trapped and are not observed to escape the plasma until the laser pulse intensity reduces. Such an effect would not impact Savin's scalings but would of course inhibit the observation of the scaling for electrons escaping to the sides and rear of the plasma block.

Returning now to figure 2.8, there are two interesting aspects. Firstly the sudden jump in total energy at $a_0 \approx 300$. This cannot be explained by ZVP theory nor QED theory since the jump is observed with QED effects switched off.

Secondly, the even sharper jump in total electron bunch energy above $a_0 = 1000$. Decomposing the total energy into bulk electrons and those produced via the BW process, this is clearly a QED effect. Energy in BW pairs scales at a staggering

$$U_{\mathrm{BW}} \sim a_0^{11.3 \pm 0.8}, \tag{2.67}$$

while energy in plasma electrons descreases. Perhaps this is a signal of Savin's QED ZVP electron bunches only at a higher energy due to the substantially greater plasma density of these simulations. Following Savin's theory,

$$U_{\mathrm{QED}} \sim \frac{a_0^7}{S}. \tag{2.68}$$

The reduction in plasma electron energy can be attributed to an oversaturation of the front surface with BW electrons. The surface now consists of mostly BW electrons. Could this replacement explain the increase in scaling observed vs the theory or can it be explained by radiation reaction or is there some other deeper effect at work?

Doubtless, the advent of next generation exa-watt scale lasers and the ability to explore this regime will be exceedingly interesting if such scalings in bunch energy can be maintained.

Discuss region of BW pair projection maximisation and where we expect saturation.

To do: Explore transition regions, do MORE simulations to fill in the gaps.

Then experiment?

Numerical heating: it is not sufficient to simply run simulations without the laser pulse to determine heating. The effect of numerical heating will be most damning for the ultra-high charge density electron bunches.

To do: convergence of electron bunch energies with nppc and sim resolution.

At aome point mention:

Note that ZVP does not describe the peak energies in the bunches, then JxB applies, since there are always some electrons outside of the well defined sharp boundary when the density is not high enough to impose adiabaticity.

3
Miscellaneous notes

Contents

3.1 ORION experiment

The following derivation determines the polarisation of the ORION laser pulses in the experiment and the boostes frame quantities for the PIC simulations.

I will have a whole subsection devoted to the different frames of reference of relevance and then a second one about normalised units. What follows now is the derivation of the boosted frame in which the laser is incident normally relative to the lab frame where the laser is incident obliquely.

I will try to use a consistent convention for coordinate system as much as possible.

3.1.1 Frames of reference

Other frames of reference include, HB front surface at rest frame, ablating front frame, smilei frames.

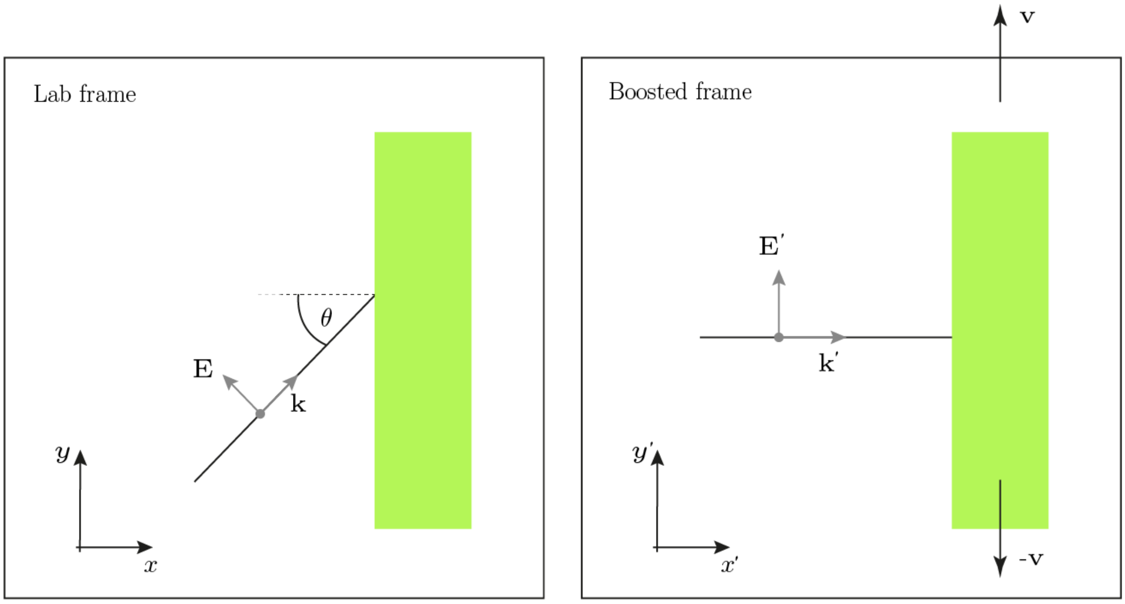

Figure 3.1

When writing out the pistoning equation in full in thesis, include analysis in Robinson 2009 to do it for multiple ion species.

I should go over this and use third year relativity notes to formalised and make more consistent.

While some of this section may seem trivial, it is frequently miscalculated in the literature, it therefore seems of great importance to provide a full derivation.

Consider a photon incident on a plasma block at angle θ as in figure 3.1. A boost is applied with velocity $\mathbf{v}$ to a frame such that the photon is normally incident on the now streaming plasma at velocity $-\mathbf{v}$. The velocity transformation for the photon's velocity, $\mathbf{u}$, parallel to the boost is

$$\mathbf{u}'_{\parallel} = \frac{\mathbf{u}_{\parallel} - \mathbf{v}}{1 - \mathbf{u}\cdot\mathbf{v}/c^2}. \tag{3.1}$$

Setting $\mathbf{u}'_{\parallel} = 0$, it is clear that

$$\mathbf{v} = \mathbf{u}_{\parallel} = c\sin\theta\hat{\mathbf{y}} \tag{3.2}$$

in this geometry and

$$\gamma_{\mathbf{v}} = \frac{1}{\sqrt{1 - \mathbf{v}^2/c^2}} = \sec\theta. \tag{3.3}$$

Noting that since Snell's law is frame invariant, the photon remains normal as it propagates into the skin depth of the plasma, a frame in which the interaction reduces to a 1D problem has been successfully found for all $\theta < \pi/2$. Those familiar with the topic may wonder how this is possible considering the 'ripples' that are observed on the plasma surface for oblique incidence. The explanation for this is of course the relativity of simultaneity. It remains to determine how do all the relevant quantities transform as such a boost is applied. Starting with an easy one: the photon's wave four-vector is

$$\mathbf{K}^{\mu} = \left(\frac{\omega}{c}, \mathbf{k}\right) \tag{3.4}$$

and thus the freqency transforms as

$$\frac{\omega}{c} = \gamma_{\mathbf{v}} \left(\frac{\omega'}{c} - \frac{\mathbf{v}}{c} \cdot \mathbf{k}'\right). \tag{3.5}$$

Since $\mathbf{v} \cdot \mathbf{k}' = 0$,

$$\omega' = \omega \cos\theta. \tag{3.6}$$

As

$$n'_{\mathrm{c}} = \frac{m_{\mathrm{e}}(\omega')^2}{4\pi e^2}, \tag{3.7}$$

$$n'_{\mathrm{c}} = n_{\mathrm{c}} \cos^2\theta, \tag{3.8}$$

while the plasma block will be Lorentz contracted along $\hat{\mathbf{y}}$, hence the number density of electrons will increase as,

$$n'_{\mathrm{e}} = \frac{n'_{\mathrm{e}}}{\cos\theta}, \tag{3.9}$$

leading to the perhaps unexpected

$$\bar{n}'_{\mathrm{e}} = \frac{\bar{n}_{\mathrm{e}}}{\cos^3\theta}. \tag{3.10}$$

Time is dilated

$$t' = \frac{t}{\cos\theta}. \tag{3.11}$$

Consider now the more general case (I should jsut simply replace my diagram with a 3D one that incorporates this initially) where the photon's electric field is rotated out of the x-y plane, *i.e.*

$$\mathbf{E} = E_0(-\cos\phi\sin\theta, \cos\phi\cos\theta, \sin\phi) \tag{3.12}$$

and correspondingly

$$\mathbf{B} = \frac{\hat{\mathbf{k}} \times \mathbf{E}}{c} = \frac{E_0}{c}(\sin\phi\sin\theta, -\sin\phi\cos\theta, \cos\phi). \tag{3.13}$$

The Lorentz transformations for electro-magnetic fields are

$$\mathbf{E}'_{\|} = \mathbf{E}_{\|}, \tag{3.14}$$

$$\mathbf{B}'_{\|} = \mathbf{B}_{\|}, \tag{3.15}$$

$$\mathbf{E}'_{\perp} = \gamma_{\mathbf{v}}(\mathbf{E}_{\perp} + \mathbf{v} \times \mathbf{B}), \tag{3.16}$$

$$\mathbf{B}'_{\perp} = \gamma_{\mathbf{v}}(\mathbf{B}_{\perp} - \mathbf{v} \times \mathbf{E}/c^2). \tag{3.17}$$

Using the above expressions for $\mathbf{E}_{\perp}$ and $\mathbf{E}_{\|}$ and transforming to the boosted frame,

$$\mathbf{E}' = E_0\cos\theta(0, \cos\phi, \sin\phi). \tag{3.18}$$

As anticipated for normal incidence there is no component of the E-field normal to the surface. Conveniently, the polarisation of the incident photon is unchanged despite having components both parallel and perpendicular to the transformation and

$$|\mathbf{E}'| = |\mathbf{E}|\cos\theta. \tag{3.19}$$

The picture can now be completed. Since

$$a'_0 = \frac{e|\mathbf{E}'|}{m_{\mathrm{e}}e\omega'} \tag{3.20}$$

it follows that

$$a'_0 = a_0, \tag{3.21}$$

$$S' = \frac{S}{\cos^3\theta}. \tag{3.22}$$

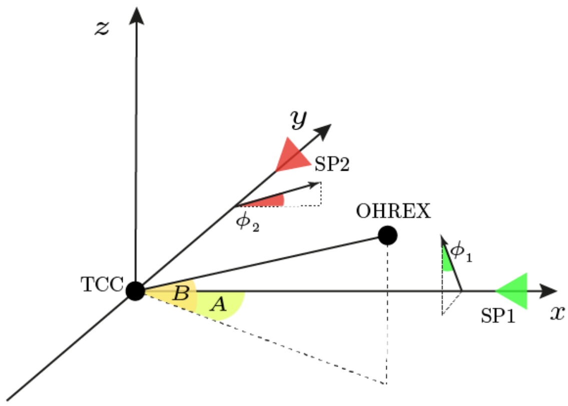

Figure 3.2: ORION target chamber geometry showing the location of the target (TCC) and OHREX spectrometer and the green (SP1) and infra-red (SP2) beamlines and their corresponding polarisations.

3.1.2 ORION interaction geometry

The ORION target chamber has its own defined geometry with the target located at the origin, described in figure 3.2. The polarisation angles are $\phi_1 = 11.8°$ and $\phi_2 = 16.4°$. Following reflection of the infra-red beam off the plasma mirror, both the green and infra-red lasers propagate in the -$\hat{\mathbf{x}}$-direction towards the origin. The OHREX crystal is located at

$$\mathbf{r}_{\mathrm{OHREX}} = r_0(\cos B \cos A, -\cos B \sin A, \sin B), \tag{3.23}$$

where $r_0 = 2.4\,\mathrm{m}$, $A = 26.82°$ and $B = 18.15°$, setting the rotation angle of the target. This was achieved using the ORION Multi-Target-Mounts. Alignment was performed by Ed Gumbrell and no further details will be provided here on that process.

The interaction plane is therefore defined by the vector

$$\mathbf{n} = \frac{\mathbf{r}_{\mathrm{OHREX}}}{r_0} \times \hat{\mathbf{x}} = (0, \sin B, \cos B \sin A). \tag{3.24}$$

The cosine rule can be applied to determine the polarisation of the laser pulses in the interaction plane, for polarisation vector $\hat{\mathbf{E}}$,

$$\frac{\mathbf{n}}{|\mathbf{n}|} \cdot \hat{\mathbf{E}} = \cos\theta, \tag{3.25}$$

where θ defines the angle between the polarisation vector and the vector normal to the interaction plane. This corresponds to angles out of the interaction plane of 42.2 or the SP1 beam (rotating anticlockwise out of the interaction plane when looking from TCC to parabola) and 19.6 or the SP2 beam (rotating clockwise out of the interaction plane when looking from TCC to parabola). Again applying the cosine rule, the angle of incidence is 16

Next up: Polarisation on OHREX interaction plane.

The same method can be applied to determine the polarisation of the OHREX crystal interaction plane. The OHREX crystals have a nominal Bragg angle of 51.3

I still need to know the exact orientation of the OHREX but assuming it is vertical, the interaction plane is defined by

$$\mathbf{n}_{\mathrm{O}} = \frac{\mathbf{r}_{\mathrm{OHREX}}}{r_0} \times \hat{\mathbf{z}} = (-\sin A, -\cos A, 0), \tag{3.26}$$

once it has been normalised.

Then again applying the cosine rule, this plane corresponds to angles out of the interaction plane of 10.5° for SP1 and 58.9° for SP2.

Is has been assumed that the non-linear RPM mechanism retains the polarisation of the incident laser pulse in the reflected harmonic beam.

Then since the OHREX crystal reflection is a linear process, we can decompose our incident beam into its polarisation constituents and consider what their combined intensity post reflection at the detector plane will be.

Also discuss the fabulous result that generally one can simply extract the results in the Smilei units and multiply by the relevant factors of the frame of interest and thus not worry too much about frame transformations.

Also check the boosted frame results against the bouchard thesis.

Once I have finished this section I must redo boosted section since I have made a mistake there and rethink a bit about optimum theta.

I must also at some point just state that a hat indicates a normalised vector.

3.1.3 Condition on validity of hole boring expression

Robinson *et al* [18] consider for what case is the expression they derive for hole boring valid. The case they are interested in is what happens if the energy available for an ion to gain from crossing the pseudo-capacitor is less than the kinetic energy associated with the hole boring velocity. Their analysis applies for non-relativistic hole boring velocities and circular polarised laser pulses. This theory is now updated for the ZVP mechanism (linear polarised and relativistic ion velocities).

The so-called 'piston' which leads to ion hole boring is the pseudocapacitor field. In section 2.2.1, the development of that field is discussed quantitatively. The peak electric field is

$$E_{\mathrm{C}} = E_{\mathrm{L}} = \sqrt{\frac{I}{\epsilon_0 c}} \tag{3.27}$$

and the peak displacement of electrons is

$$\Delta x = \frac{\epsilon_0 E_{\mathrm{C}}}{e n_{\mathrm{e}}}. \tag{3.28}$$

Considering instead the relativistic kinetic energy gained by an ion were it to fully cross the pseudocapacitor, following equation 2.28,

$$T_i = Z_i \times \frac{1}{2} m_{\mathrm{e}} c^2 \frac{a_0^2}{\bar{n}_{\mathrm{e}}} = \frac{I Z_i}{2 c n_m athrme}. \tag{3.29}$$

(The equation above needs more thinking about)

Ions are reflected provided,

$$T_i > \frac{1}{2} m_i v_{\mathrm{HB}}^2. \tag{3.30}$$

Hmm ok so in Vincenti, they approximate electron mass as much less than ion mass and therefore neglect in the momentum calculation. It also looks like they have not done full relativistic calculation, so I cannot yet say I have that. But carrying on the derivation using Vincenti expression for simplicity:

The hole-boring velocity as calculated by Vincenti *et al* [12] is

$$\frac{v_{\mathrm{HB}}}{c} = \sqrt{\frac{R \cos \theta}{2}} \tag{3.31}$$

So come back to this section, once I have fully written out the hole boring calcualtino in full, include also the multiple ion species stuff and this condition.

The upshot of this condition is something like: require no low charge to mass ratio ions (ie v heavy ions) and fully ionisation, these conditions are satisfied in this area of study.

To arrive at that result, useful parts include: composite mass density $\rho = \sum_i m_i n_i$, $m_i = A_i / N_\mathrm{A}$ and $A_i \approx 2Z_i$ for most low mass ions relevant in these plasmas.

Appendices

Cor animalium, fundamentum eft vitæ, princeps omnium, Microcofmi Sol, a quo omnis vegetatio dependet, vigor omnis & robur emanat.

The heart of animals is the foundation of their life, the sovereign of everything within them, the sun of their microcosm, that upon which all growth depends, from which all power proceeds.

— William Harvey [**harvey_exercitatio_1628**]

A
General plasma physics

Contents

A.1 The headlight effect

The headlight effect describes the beaming of an isotropically emitting source travelling at some velocity relative to an observer. Consider the geometry of figure 2.2 with the source (the laser pulse) travelling at an angle 2θ to the observer (in this case, the ablating front). A photon with energy E emitted from the rest frame of the source (the laboratory frame in this case) has a 4-momentum

$$\mathbf{P}_\mu = \left(\frac{E}{c}, \frac{E}{c}\cos 2\theta, \frac{E}{c}\sin 2\theta\right). \tag{A.1}$$

As the interaction geometry is confined to a 2D plane, the z-component can be safely neglected. Applying the lorentz boost of equation 2.12,

$$\begin{aligned} \frac{E'}{c} &= \gamma\left(\frac{E}{c} - \beta\frac{E}{c}\cos 2\theta\right) \\ \frac{E'}{c}\cos 2\theta' &= \gamma\left(\frac{E}{c}\cos 2\theta - \beta\frac{E}{c}\right). \end{aligned} \tag{A.2}$$

Solving these equations for the angle in the boosted frame,

$$\cos 2\theta' = \frac{\cos 2\theta - \beta}{1 - \beta \cos 2\theta}. \tag{A.3}$$

A.2 Geometric transverse emittance

A beam[1] of particles is fully described by its six-dimensional particle phase space distribution

$$\rho(\mathbf{x}, \mathbf{p}) = \rho(x, p_x, y, p_y, z, p_z), \tag{A.4}$$

where $\mathbf{p} = p_x\hat{\mathbf{x}} + p_y\hat{\mathbf{y}} + p_z\hat{\mathbf{z}}$ is the canonical momentum [**mcDonald Methods of emittance measurem 1989**]. Under the Hamilton formalism, for ideal conditions, the six-dimensional volume of the beam in this space, termed the *emittance*, arises as a conserved quantity and is therefore a useful quantity to describe the beam quality. (something to do with it affecting the ability to focus the beam?? check the papers) It is useful to rotate the coordinate system so as to align with the beam's propagation. The distribution can be written as

$$\rho(\mathbf{x}', \mathbf{p}') = \rho(x_{\mathrm{L}}, p_{\mathrm{L}}, x_{\mathrm{T}}, p_{\mathrm{T}}, x_{\mathrm{T}'}, p_{\mathrm{T}'}), \tag{A.5}$$

where L is longitudinal to the beam's propagation direction, and T and T′ are two orthogonal directions transverse to the beam's propagation. Where discussed in this thesis, T′ will unanimously refer to the z-direction, that is, the additional direction in 3D simulations, all such simulations are designed such that the z-direction is transverse to the beam propagation direction.

Recording a six-dimensional phase space in experiment is impossible while in simulations it is almost prohibitively costly in terms of data storage. Hence, it is common practice to project the distribution onto three orthogonal sub-spaces corresponding to each spatial axis, L, T and T′ and compute the area on each. Note that since the electron beam is ultra-relativistic, all electrons propagate at approximately c and therefore it is the transverse and not the longitudinal emittance

[1] In this section it is electron beams and not bunches that a referred to to demonstrate the generality of these concepts.

that describes the beam's quality. As a particle beam does not typically exist with well-defined borders, the area used to describe the emittance is restricted to an ellipse containing only the high-density core of the distribution. For a subspace i, where $i = \mathrm{T}$ or T', Floettmann *et al* [19] derive the *transverse normalised emittance* as

$$\epsilon^i_{\mathrm{n,rms}} = \frac{1}{m_\mathrm{e}c}\sqrt{\langle x_i^2\rangle\langle p_i^2\rangle - \langle x_i p_i\rangle^2}, \tag{A.6}$$

where $\langle\rangle$ is the second central moment of the particle distribution,

$$\langle ab\rangle = \frac{\int ab\rho(\mathbf{x}',\mathbf{p}')dV}{\int \rho(\mathbf{x}',\mathbf{p}')dV} - \frac{\int a\rho(\mathbf{x}',\mathbf{p}')dV \int a\rho(\mathbf{x}',\mathbf{p}')dV}{(\int \rho(\mathbf{x}',\mathbf{p}')dV)^2}, \tag{A.7}$$

here $dV = \Pi_j dx_j dp_j$ for $j =$L, T, T$'$.

When working with emittances, most frequently in the literature it is the *transverse geometric emittance*, $\epsilon^i_{\mathrm{rms}}$ that is discussed. This is a natural consequence of it being more readily accessible in experiments [**mcDonald Methods of emittance measuremen 1989**]. The geometric and normalised emittances are related via

$$\epsilon^i_{\mathrm{rms}} = \frac{\epsilon^i_{\mathrm{rms}}}{\gamma\beta_\mathrm{L}}, \tag{A.8}$$

where $\gamma = 1/\sqrt{1-\beta^2}$ refers to the beam's mean energy and $\beta_\mathrm{L} \approx c$ is the ultrarelativistic beam's longitudinal speed.

The Courant-Snyder invariant which describes the ellipse that corresponds to the emittance is[2]

$$\epsilon^i_{\mathrm{rms}} = \gamma x_i^2 + 2\alpha x x'\beta x_i'^2, \tag{A.9}$$

here the coordinates are x_i and $x_i' = p_i/p_\mathrm{L}$ [20]. The Twiss parameters are

$$\alpha = -\frac{\langle x_i x_i'\rangle}{\epsilon^i_{\mathrm{rms}}}, \tag{A.10}$$

$$\beta = \frac{\langle x_i\rangle}{\epsilon^i_{\mathrm{rms}}} \tag{A.11}$$

and

$$\gamma = \frac{\langle x_i'^2\rangle}{\epsilon^i_{\mathrm{rms}}}. \tag{A.12}$$

Thus the shape of the ellipse and the divergence of the beam can be determined.

[2]Regrettably β and γ are the standard notations for the Twiss parameters, at all other locations in this thesis, these parameters will refer to the standard relativistic beta and gamma factors of objects respectively.

The first kind of intellectual and artistic personality belongs to the hedgehogs, the second to the foxes …

— Sir Isaiah Berlin [**berlin_hedgehog_2013**]

References

[1] Herbert Goldstein. *Classical Mechanics*. Pearson Education, 2013.

[2] Igor V. Sokolov et al. "Dynamics of Emitting Electrons in Strong Electromagnetic Fields". In: *Physics of Plasmas* 16.9 (Sept. 1, 2009), p. 093115. arXiv: 0904.0405 [physics]. URL: http://arxiv.org/abs/0904.0405 (visited on 08/01/2023).

[3] J. Derouillat et al. "Smilei : A Collaborative, Open-Source, Multi-Purpose Particle-in-Cell Code for Plasma Simulation". In: *Computer Physics Communications* 222 (Jan. 2018), pp. 351–373. URL: https://linkinghub.elsevier.com/retrieve/pii/S0010465517303314 (visited on 08/15/2023).

[4] *ARCHER2*. URL: https://www.archer2.ac.uk/ (visited on 08/15/2023).

[5] T. Baeva et al. "The Zero Vector Potential Mechanism of Attosecond Absorption". In: *Physics of Plasmas* 18.5 (May 2011).

[6] A. F. Savin et al. "Attosecond-Scale Absorption at Extreme Intensities". In: *Physics of Plasmas* 24.11 (Nov. 1, 2017).

[7] Alex Savin. "Modelling Laser-Plasma Interactions for the Next Generation of High-Power Laser Experiments". In: (2019).

[8] S C Wilks et al. *Absorption of Ultra-Intense Laser Pulses*. 1992.

[9] A. A. Gonoskov et al. "Ultrarelativistic Nanoplasmonics as a Route towards Extreme-Intensity Attosecond Pulses". In: *Physical Review E* 84.4 (Oct. 10, 2011), p. 046403. URL: https://link.aps.org/doi/10.1103/PhysRevE.84.046403 (visited on 07/24/2023).

[10] Andrew M. Steane. *Relativity Made Relatively Easy*. OUP Oxford, Oct. 4, 2012. 437 pp. Google Books: 75rCErZkh7EC.

[11] T. Baeva, S. Gordienko, and A. Pukhov. "Theory of High-Order Harmonic Generation in Relativistic Laser Interaction with Overdense Plasma". In: *Physical Review E - Statistical, Nonlinear, and Soft Matter Physics* 74.4 (2006). arXiv: physics/0604228.

[12] H. Vincenti et al. "Optical Properties of Relativistic Plasma Mirrors". In: *Nature Communications* 5 (Mar. 11, 2014). pmid: 24614748.

[13] K. A. Tanaka et al. "Current Status and Highlights of the ELI-NP Research Program". In: *Matter and Radiation at Extremes* 5.2 (Mar. 1, 2020), p. 024402. URL: https://pubs.aip.org/mre/article/5/2/024402/253013/Current-status-and-highlights-of-the-ELI-NP (visited on 08/31/2023).

[14] A. Bret, L. Gremillet, and M. E. Dieckmann. “Multidimensional Electron Beam-Plasma Instabilities in the Relativistic Regime”. In: *Physics of Plasmas* 17.12 (Dec. 1, 2010), p. 120501. URL: `https://pubs.aip.org/pop/article/17/12/120501/919014/Multidimensional-electron-beam-plasma` (visited on 08/31/2023).

[15] Alex F. Savin et al. “Energy Absorption in the Laser-QED Regime”. In: *Scientific Reports* 9.1 (Dec. 1, 2019). pmid: `31222083`.

[16] M. Thévenet et al. “Vacuum Laser Acceleration of Relativistic Electrons Using Plasma Mirror Injectors”. In: *Nature Physics* 12.4 (Apr. 1, 2016), pp. 355–360. arXiv: `1511.05936`.

[17] L. L. Ji et al. “Radiation-Reaction Trapping of Electrons in Extreme Laser Fields”. In: *Physical Review Letters* 112.14 (Apr. 8, 2014), p. 145003. URL: `https://link.aps.org/doi/10.1103/PhysRevLett.112.145003` (visited on 09/07/2023).

[18] A. P.L. Robinson, D. H. Kwon, and K. Lancaster. “Hole-Boring Radiation Pressure Acceleration with Two Ion Species”. In: *Plasma Physics and Controlled Fusion* 51.9 (2009).

[19] Klaus Floettmann. “Some Basic Features of the Beam Emittance”. In: *Physical Review Special Topics - Accelerators and Beams* 6.3 (2003), pp. 80–86.

[20] wiedemann. *Particle Accelerator Physics*. New York, NY: Springer Berlin Heidelberg, 2015.